MCB
Journals.ASM.org

Targeting SQSTM1/p62 Induces Cargo Loading Failure and Converts Autophagy to Apoptosis via NBK/Bik

Shuang Chen,[a] Liang Zhou,[a] Yu Zhang,[a,b] Yun Leng,[a,c] Xin-Yan Pei,[a] Hui Lin,[a] Richard Jones,[d] Robert Z. Orlowski,[d] Yun Dai,[a] Steven Grant[a,e]

Department of Medicine, Virginia Commonwealth University and Massey Cancer Center, Richmond, Virginia, USA[a]; National Engineering Laboratory for Druggable Gene and Protein Screening, Northeast Normal University, Changchun, Jilin, China[b]; Department of Hematology, Beijing Chaoyang Hospital of Capital Medical University, Beijing, China[c]; Department of Lymphoma and Myeloma, University of Texas M. D. Anderson Cancer Center, Houston, Texas, USA[d]; Department of Biochemistry, Virginia Commonwealth University and Massey Cancer Center and Virginia Institute of Molecular Medicine, Richmond, Virginia, USA[e]

In selective autophagy, the adaptor protein SQSTM1/p62 plays a critical role in recognizing/loading cargo (e.g., malfolded proteins) into autophagosomes for lysosomal degradation. Here we report that whereas SQSTM1/p62 levels fluctuated in a time-dependent manner during autophagy, inhibition or knockdown of Cdk9/cyclin T1 transcriptionally downregulated SQSTM1/p62 but did not affect autophagic flux. These interventions, or short hairpin RNA (shRNA) directly targeting SQSTM1/p62, resulted in cargo loading failure and inefficient autophagy, phenomena recently described for Huntington's disease neurons. These events led to the accumulation of the BH3-only protein NBK/Bik on endoplasmic reticulum (ER) membranes, most likely by blocking loading and autophagic degradation of NBK/Bik, culminating in apoptosis. Whereas NBK/Bik upregulation was further enhanced by disruption of distal autophagic events (e.g., autophagosome maturation) by chloroquine (CQ) or Lamp2 shRNA, it was substantially diminished by inhibition of autophagy initiation (e.g., genetically by shRNA targeting Ulk1, beclin-1, or Atg5 or pharmacologically by 3-methyladenine [3-MA] or spautin-1), arguing that NBK/Bik accumulation stems from inefficient autophagy. Finally, NBK/Bik knockdown markedly attenuated apoptosis *in vitro* and *in vivo*. Together, these findings identify novel cross talk between autophagy and apoptosis, wherein targeting SQSTM1/p62 converts cytoprotective autophagy to an inefficient form due to cargo loading failure, leading to NBK/Bik accumulation, which triggers apoptosis.

Autophagy is an evolutionarily conserved process by which damaged organelles and unneeded proteins are degraded by lysosomes to maintain intracellular homeostasis and to recycle cellular nutrients. While autophagy can promote cell death (1), in most cases, it is cytoprotective and contributes to drug resistance (2). In response to chemotherapeutic agents, apoptosis (type I) and autophagy (type II) represent two major forms of programmed cell death (3). Autophagy and apoptosis share molecular regulatory mechanisms governed by Bcl-2 family proteins (3, 4). Specifically, Bcl-2 and Bcl-x_L prevent both apoptosis and autophagy by sequestering different BH3-only proteins (e.g., proapoptotic Bim and Bid [5] and proautophagic beclin-1 [6, 7]). As a result, antagonism of Bcl-2/Bcl-x_L function releases and activates these BH3-only proteins, leading to apoptosis and autophagy, respectively (8). While apoptosis represents a well-established mechanism of action of conventional and targeted anticancer agents (3), autophagy may play both positive and negative roles in tumorigenesis and cancer treatment (9, 10). Consequently, whether autophagy should be inhibited or activated remains the subject of debate. Accordingly, both autophagy inhibitors and inducers are currently undergoing clinical evaluation (11).

Protection of cells from injury by harmful macromolecules or damaged organelles through autophagy as a quality control (QC) mechanism (11, 12) involves the sequestration and transport of cellular constituents to lysosomes for degradation (13). Autophagy is initiated by phagophore formation (initiation/nucleation stage), followed by the development of a crescent-shaped double membrane that expands and fuses to form a double-membrane vesicle known as an autophagosome (elongation stage). The autophagosome then fuses with lysosomes to form autolysosomes (maturation stage), resulting in the degradation of vacuolar content (13). Recent evidence indicates that autophagy is a more selective process than originally thought (14–16). Selective autophagy depends on the binding of substrates to the inner surface of the growing phagophore (17), referred to as cargo loading (18), a process mediated by adaptor proteins (19) associated with both the substrate (cargo recognition) and lipidated LC3 anchored to the phagophore (20, 21). p62, also known as sequestosome 1 (SQSTM1), is selectively degraded by autophagy (22, 23) and serves as a key cargo adaptor for the degradation of ubiquitinated substrates (22, 24–26). Thus, p62 plays a central role in selective autophagy involving the clearance of malfolded (e.g., unfolded or misfolded) proteins (20, 25), protein aggregates/aggresomes (22), ubiquitin-labeled peroxisomes (27), and Parkin-labeled mitochondria (24).

Inefficient autophagy resulting from cargo recognition failure has recently been implicated in Huntington's disease (28), a neurodegenerative disorder caused by macroautophagy malfunction

Received 17 October 2013 **Returned for modification** 29 December 2013
Accepted 22 June 2014
Published ahead of print 7 July 2014
Address correspondence to Yun Dai, ydai@vcu.edu, or Steven Grant, stgrant@vcu.edu.
S.C. and L.Z. contributed equally to this work.
Supplemental material for this article may be found at http://dx.doi.org/10.1128/MCB.01383-13.

doi:10.1128/MCB.01383-13

and accumulation of the neurotoxic huntingtin protein (htt) (28, 29). Inefficient autophagy has been defined as autophagy in which autophagic vacuoles (AVs) fail to trap cytosolic cargo despite their formation at normal or even enhanced rates and adequate lysosomal elimination (28). In this context, the autophagic adaptor protein SQSTM1/p62 acts to recognize ubiquitinated protein aggregates and link them, through binding to LC3, to autophagosomes, a cargo loading process necessary for lysosomal degradation during selective autophagy. We therefore hypothesized that targeting the cargo loading protein p62 in neoplastic cells might lead to cargo loading failure and, as a consequence, inefficient autophagy, which could be exploited to promote apoptosis.

MATERIALS AND METHODS

Cells and reagents. Human multiple myeloma U266 and RPMI8226 cells were obtained from the ATCC and maintained as described previously (5), and both cell lines were authenticated (Basic STR Profiling Service, ATCC 135-X) by the ATCC before this study was completed. Bortezomib-resistant cells (PS-R) were generated by continuously culturing U266 cells in increasing concentrations of bortezomib (beginning at 0.5 nM and increasing in stepwise increments of 0.2 nM) up to 20 nM and were maintained in medium containing 15 nM bortezomib. U266/Mcl-1, U266/Bcl-2, RPMI8226/Bcl-x_L, and U266/DN-caspase 9 cells were established by stably transfecting human full-length Mcl-1, Bcl-2, and Bcl-x_L cDNAs and dominant negative caspase 9 (287 cysteine→alanine), respectively. All experiments utilized logarithmically growing cells (3×10^5 to 5×10^5 cells/ml). Wild-type (wt) and p62 gene knockout (ko) mouse embryonic fibroblasts (MEFs) as well as the pEGFP-p62 plasmid were kindly provided by Jorge Moscat (Sanford-Burnham Medical Research Institute) (30).

The pan-BH3 mimetic GX-015-070 (GX) (obatoclax) was provided by Teva Pharmaceuticals (North Wales, PA) in association with the Cancer Treatment and Evaluation Program (CTEP) of the NCI. The pan-Cdk inhibitors flavopiridol (FP) (alvocidib; Sanofi-Aventis, Bridgewater, NJ) and SCH727965 (dinaciclib; Merck, Whitehouse Station, NJ) were provided by the NCI. The proteasome inhibitor bortezomib (Velcade) was provided by Millennium (Cambridge, MA). Cycloheximide (CHX) and MG-132 were purchased from Sigma (St. Louis, MO) and Calbiochem (San Diego, CA), respectively; dissolved in dimethyl sulfoxide (DMSO); aliquoted; and stored at −20°C. In all experiments, final DMSO concentrations did not exceed 0.1%. If not indicated specifically, the time of drug treatment was 24 h.

Flow cytometry. The extent of apoptosis was evaluated by flow cytometry utilizing annexin V-fluorescein isothiocyanate (FITC)-propidium iodide (PI) (5). Briefly, 1×10^6 cells were stained with annexin V-FITC (BD PharMingen, San Diego, CA) and 5 μg/ml PI (Sigma) in 1× binding buffer for 15 min at room temperature in the dark. Samples were then analyzed by BD Biosciences FACSCalibur flow cytometry (Becton, Dickinson, San Jose, CA) within 1 h to determine the percentage of apoptotic (annexin V-positive) cells.

TUNEL analysis. In some cases, cytospin slides were stained for terminal deoxynucleotidyltransferase-mediated dUTP-biotin nick end labeling (TUNEL) by using an In Situ Cell Death Detective kit (fluorescein; Roche, Penzberg, Germany) according to the manufacturer's instructions. Images were captured by using an Olympus BX40 fluorescence microscope at 20×/0.50 numerical aperture (Olympus America Inc., Center Valley, PA) and a CE digital camera (Alpha Innotech Corp., San Leandro, CA) with RS Image software version 1.7.3 (Roper Scientific Photometrics, Tucson, AZ).

Immunofluorescence. Ubiquitin-positive protein aggregates were examined by immunofluorescence using an antiubiquitin monoclonal antibody (Cell Signaling, Beverly, MA), as reported previously (31). Images were captured by using a Zeiss LSM 700 confocal laser scanning microscope.

Autophagy analysis. Autophagy analysis was performed as follows. (i) Whole-cell lysates were prepared and subjected to immunoblot analysis using an anti-LC3 antibody (Novus, Littleton, CO) to monitor LC3 processing from LC3-I to LC3-II. To exclude the possibility that increases in LC3-II levels reflect reduced autophagic degradation rather than enhanced induction, analysis of autophagic flux was performed by using bafilomycin A1 as previously described (32, 33). (ii) An expression construct encoding the enhanced green fluorescent protein (EGFP)-LC3B fusion protein (Addgene plasmid 11546) was obtained from Addgene (Cambridge, MA) (34). Autophagy was visualized in U266 and PS-R cells by stable transfection with pEGFP-LC3B followed by observation of LC3 puncta using a confocal microscope. (iii) Electron microscopy (EM) was employed to analyze ultrastructural morphology of autophagy by using a JEOL JEM-1230 transmission electron microscope. (iv) Autophagic flux was validated by transient transfection of cells with a pBABE-puro mCherry-EGFP-LC3B plasmid (Addgene plasmid 22418) (35), followed by observation of autophagosomes (mCherry and green fluorescent protein [GFP] double positive [yellow]) and autolysosomes (mCherry only [red]) using a confocal microscope.

Lysosome analysis. To monitor lysosome mass and number, cytospin slides were stained for lysosomes by using a LysoTracker probe (Molecular Probes by Life Technology, Carlsbad, CA) according to the manufacturer's instructions. Images were captured by using a confocal microscope.

Filter trap (retardation) assay. Protein aggregates were assessed by using a filter trap assay as described previously (12, 36). Briefly, cells were lysed in 1× phosphate-buffered saline (PBS) containing 1 mM phenylmethylsulfonyl fluoride (PMSF) by sonication for 1 min. Total protein was quantified by using Coomassie protein assay reagent (Pierce, Rockford, IL). Equal amounts of protein (10 μg) were diluted in 1% SDS and filtered through a cellulose acetate membrane (0.2-μm pore size; Whatman, Dassel, Germany) by using a dot microfiltration (Bio-Rad, Hercules, CA) or slot blotting (Hoefer, San Francisco, CA) apparatus. The membrane was washed with 1× PBS containing 1% SDS, followed by blocking with 5% skim milk in 1× PBS. The SDS-insoluble aggregates trapped on the filter were probed with antiubiquitin (Cell Signaling, Beverly, MA), anti-p62 (Santa Cruz Biotechnology, Santa Cruz, CA), or anti-Bik (ProSci, Poway, CA).

Quantitative real-time PCR. Quantitative real-time PCR (qPCR) analysis using TaqMan gene expression assays and a 7900HT real-time PCR system (Applied Biosystems, Foster City, CA) was performed to quantify mRNA levels of human NBK/Bik and SQSTM1/p62 (5). Briefly, total RNA was isolated by using TRIzol reagent (Invitrogen, Carlsbad, CA) according to the manufacturer's instructions. Genomic DNA was digested with DNase I (amplification grade; Invitrogen). cDNA was synthesized from 1 μg of total RNA by using a High Capacity cDNA reverse transcription kit (Applied Biosystems). Two microliters of cDNA was employed for qPCR assays (TaqMan gene expression assays). Assay identification numbers for NBK/Bik and SQSTM1/p62 were Hs00154189_m1 and Hs01061917_g1, respectively. References for quantitation were human β-actin and glyceraldehyde-3-phosphate dehydrogenase (GAPDH) (predeveloped TaqMan assay reagent control kit; Applied Biosystems). Data were analyzed by using SDS 2.3 software.

Immunoblotting. Whole-cell pellets were lysed by sonication in 1× sample buffer (62.5 mM Tris base [pH 6.8], 2% SDS, 50 mM dithiothreitol [DTT], 10% glycerol, 0.1% bromphenol blue, and 5 μg/ml each of chymostatin, leupeptin, aprotinin, pepstatin, and soybean trypsin inhibitor) and boiled for 5 min. Total protein was quantified by using Coomassie protein assay reagent (Pierce, Rockford, IL). Equal amounts of protein (30 μg) were subjected to immunoblotting according to procedures described previously (5). Where indicated, the blots were reprobed with antibodies against β-actin (Sigma) or α-tubulin (Oncogene, La Jolla, CA) to ensure equal loading and transfer of proteins. The following antibodies were used as primary antibodies: anti-Bik and anti-Bim (ProSci); anti-caspase 3, anti-Mcl-1, and anti-cytochrome *c* (BD PharMingen); anti-cleaved

caspase 3 (Asp175), anti-cleaved poly(ADP-ribose) polymerase (PARP) (Asp214), anti-SQSTM1/p62, antiubiquitin, anti-Bcl-x_L, and anti-beclin-1 (Cell Signaling); anti-human Bcl-2 oncoprotein (Dako, Carpinteria, CA); anti-PARP (Biomol, Plymouth Meeting, PA); and anti-Bik, anti-LAMP2, anti-ULK1, anti-ATG5, anti-AIF, anti-Bax, and anti-Bak (Santa Cruz Biotechnology, Santa Cruz, CA).

Immunoprecipitation. (Co)immunoprecipitation analysis was performed to evaluate ubiquitination of NBK/Bik or interactions of beclin-1 with Bcl-2, Bcl-x_L, and Mcl-1 (5). For these studies, CHAPS buffer {150 mM NaCl, 10 mM HEPES (pH 7.4), protease inhibitors, and 1% 3-[(3-cholamidopropyl)-dimethylammonio]-1-propanesulfonate (CHAPS)} was employed to avoid artifactual associations reported for buffers containing other detergents (e.g., NP-40 or Triton X-100). Briefly, cells were lysed in CHAPS buffer, and 200 μg of protein per condition was incubated with 1 μg anti-Bik (Santa Cruz Biotechnology), anti-Bcl-2 (Dako), anti-Bcl-x_L (Cell Signaling), or anti-Mcl-1 (BD PharMingen) overnight at 4°C. Twenty microliters of Dynabeads (Dynal, Oslo, Norway) per condition was then added, and the mixture was incubated for an additional 4 h. After washing, the bead-bound protein was eluted by vortexing and boiling in 20 μl 1× sample buffer. The samples were separated by SDS-PAGE and subjected to immunoblot analysis as described above. Antiubiquitin (Cell Signaling) and anti-beclin-1 (Santa Cruz) were used as primary antibodies.

Endoplasmic reticulum isolation. The endoplasmic reticulum (ER) fraction was isolated from cultured cells by using an Endoplasmic Reticulum Isolation kit (Sigma) according to the manufacturer's instructions and subjected to immunoblotting using anti-Bik antibody (ProSci) to determine the subcellular localization of NBK/Bik. The blots were reprobed with antibodies against calnexin (an ER membrane marker) (Abcam, Cambridge, MA) as a loading control.

Mitochondrion isolation. The mitochondrial fraction was isolated from cultured cells by using a Mitochondria Isolation kit (Sigma) according to the manufacturer's instructions and subjected to immunoblotting using anti-Bik and anti-Bim antibodies (ProSci) to compare subcellular localizations of Bik and Bim. The blots were reprobed with antibodies against Bak (a mitochondrial membrane marker) (Santa Cruz) as a loading control.

RNA interference. SureSilencing short hairpin RNA (shRNA) plasmids (neomycin resistance) were purchased from SABioscience (Frederick, MD), which include shRNAs targeting SQSTM1 (GenBank accession number NM_003900; clone 4 [ACTGGACCCATCTGTCTTCAA]), Ulk1 (accession number NM_003565; clone 3 [TACACGCCATCTCCTCAAGTT]), Bik (accession number NM_001197; clone 3 [CACACTTAAGGAGAACATAAT]), Atg5 (accession number NM_004849; clone 3 [TCATGGAATTGAGCCAATGTT]), BECN1 (accession number NM_003766; clone 2 [CCATGCTCTGGCCAATAAGAT]), Cdk9 (accession number NM_001261; clone 1 [GGTCAAGTTCACGCTGTCTGA]), and CCNT1 (accession number NM_001240; clone 4 [TCGTGTCCCTCATTCGAAACT]) and a scrambled sequence as a control (GGAATCTCATTCGATGCATAC). U266 cells were stably transfected with these constructs by using an Amaxa Nucleofector device with Cell Line Specific Nucleofector kit C (Amaxa GmbH, Cologne, Germany) according to the manufacturer's instructions (5). The Lentiviral Particle Gene Silencers construct (sc-29390-V) encoding shRNA targeting human Lamp2 and control lentiviral particles were purchased from Santa Cruz Biotechnology (Santa Cruz, CA) and used to transduce RPMI8226 cells. For all shRNA experiments, four constructs encoding shRNAs designed specifically against different sequences of the target gene of interest were obtained and tested before use. Subsequently, at least two constructs displaying the most pronounced knockdown of target expression were selected, validated, and employed in experiments. Stable clones with downregulated expression of the targeted genes were selected with 400 μg/ml G418 or 2 μg/ml puromycin.

Animal studies. These studies were approved by the Virginia Commonwealth University IACUC and performed in accordance with guidelines of the U.S. Department of Agriculture, the U.S. Department of Health and Human Services, and the NIH. Three mouse models were employed in this study, as reported previously (5), including (i) athymic NCr-nu/nu mice (Jackson Laboratories, Bar Harbor, ME) subcutaneously inoculated in the flank with 5×10^6 RPMI8226 cells, (ii) NOD/SCID/gamma (NSG) mice (Jackson Laboratories) subcutaneously inoculated in two side flanks with 1×10^7 U266 cells expressing Bik (right) or scrambled sequence shRNA (left), and (iii) NSG mice intravenously (i.v.) injected with 5×10^6 U266 cells stably expressing luciferase. GX-015-070 was freshly reconstituted with 5% dextrose for injection (USP) and administered via intramuscular or intraperitoneal (i.p.) injection. FP in DMSO was diluted in 0.9% saline and administered via i.p. injection. Control animals were injected with equal volumes of vehicle. Mice were monitored for tumor growth every other day visually or with the use of an Ivis 200 imaging system (Xenogen Corp., Alameda, CA).

Statistical analysis. Values represent the means ± standard deviations (SD) for at least three independent experiments performed in triplicate. The significance of differences between experimental variables was determined by using a two-tailed Student *t* test. A P value of <0.05 was considered significant.

RESULTS

Cdk inhibitors convert BH3 mimetic-induced autophagy to apoptosis. BH3 mimetics induce autophagy by dissociating beclin-1 from Bcl-2 (7), whereas coadministration of Cdk (cyclin-dependent kinase) inhibitors, which inhibit transcriptional Cdks (e.g., Cdk9), strikingly increase apoptosis (5). The question of whether Cdk inhibitors might affect BH3 mimetic-induced autophagy in human multiple myeloma (MM), a disease of malignant plasma cells, which rely on the clearance of excess immunoglobulins to maintain homeostasis necessary for survival (37), was first examined. The BH3 mimetic GX-015-070 (GX) (also known as obatoclax) as well as the anti-MM agent bortezomib, which is known to induce autophagy in MM cells (37), sharply induced autophagy, reflected by a striking increase in the level of LC3-II, a marker of autophagy (32, 33, 38), in U266 cells (Fig. 1A, left), their bortezomib-resistant counterparts (PS-R) (see Fig. S1A in the supplemental material), and RPMI8226 cells (see Fig. S1B in the supplemental material). Consistent with these findings, exposure to GX also resulted in a marked increase in the number of GFP-LC3 puncta (Fig. 1A, right). Significantly, this phenomenon was accompanied by a pronounced activation of apoptosis, reflected by cleavage of caspases 3, 8, and 9 (see Fig. S1C in the supplemental material) and PARP (Fig. 1A; see also Fig. S1A and B in the supplemental material) as well as increased TUNEL positivity (Fig. 1B). Autophagy induction was associated with the release of beclin-1 from Bcl-2 and Bcl-x_L (see Fig. S1D in the supplemental material). The Cdk inhibitor flavopiridol (FP) did not affect GX-induced LC3-II expression but clearly increased numbers of GFP-LC3 puncta compared to GX alone (Fig. 1A; see also Fig. S1A in the supplemental material). Moreover, analysis of autophagic flux demonstrated that when autophagic degradation was blocked by bafilomycin A1, an agent that inhibits the vacuolar-type H^+-ATPase complex necessary for lysosomal acidification (32, 33), treatment with either GX or GX plus FP further increased LC3-II levels in U266 cells ($P < 0.05$ versus bafilomycin A1 alone) (Fig. 1C). Furthermore, coadministration of GX with FP increased both autophagosome (yellow) and autolysosome (red) levels in U266 cells transiently transfected with mCherry-GFP LC3 (Fig. 1D). These findings support the notion that FP does not affect autophagic flux (including autophagosome formation and maturation) in cells exposed to GX.

To further explore the role of FP in the responses of MM cells

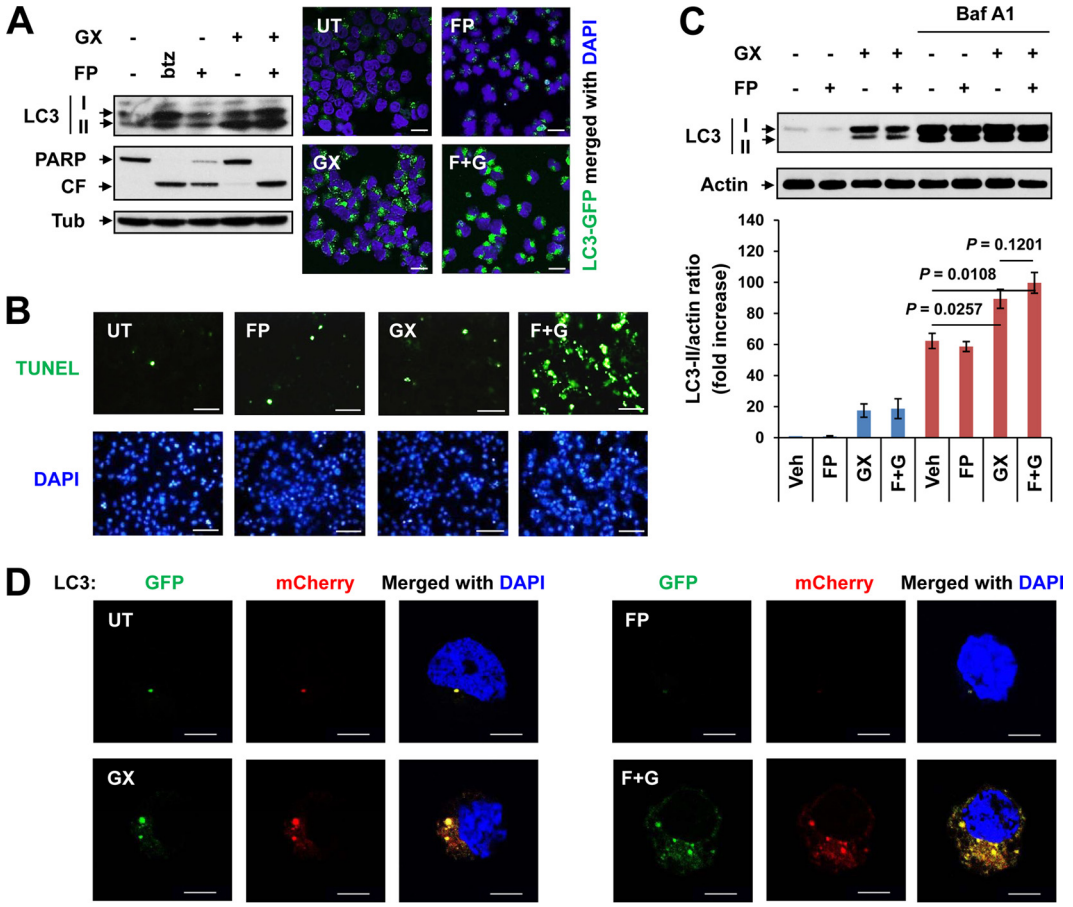

FIG 1 BH3 mimetics induce autophagy and apoptosis in the presence of Cdk inhibitors. (A) Human myeloma U266 cells were exposed to 500 nM GX-015-070 (GX) with or without 100 nM flavopiridol (FP) or 4 nM bortezomib (btz) as a positive control, followed by immunoblot analysis for LC3 (16 h) and PARP cleavage (24 h). In parallel, U266 cells were stably transfected with pEGFP-LC3, followed by exposure (16 h) to 500 nM GX with or without 100 nM FP, and then analyzed for GFP-LC3 puncta by confocal microscopy (bar = 10 μm). F+G, FP plus GX; CF, cleaved fragment; UT, untreated; DAPI, 4′,6-diamidino-2-phenylindole. (B) U266 cells were exposed (24 h) to 500 nM GX with or without 100 nM FP, followed by TUNEL staining using fluorescence microscopy (bar = 40 μm). (C) U266 cells were treated (16 h) with 500 nM GX with or without 100 nM FP in the presence or absence of 10 nM bafilomycin A1 (Baf A1), followed by analysis of autophagic flux by immunoblotting for LC3 (top). LC3-II was quantified relative to actin levels (bottom). Results represent fold increases over the vehicle-treated control (Veh) (means ± SD for three experiments). (D) Alternatively, U266 cells were transiently transfected with a pBABE-puro mCherry-EGFP-LC3B plasmid. After 6 h, cells were treated with 500 nM GX with or without 100 nM FP for an additional 16 h, followed by analysis of autophagic flux by confocal microscopy (bar = 5 μm).

to GX, cells were examined by electron microscopy (EM) (Fig. 2A). GX induced striking increases in the numbers of double-membraned autophagosomes and autolysosomes containing identifiable cellular organelles such as deformed mitochondria (Fig. 2A, bottom, high magnification). Notably, whereas FP-GX cotreatment modestly increased the number of vacuolated structures, higher magnification revealed that most vesicles were double-membraned autophagic vacuoles (AVs), which appeared empty (i.e., exhibiting clear content). The double membrane and clear content of the cytosolic vacuoles were analogous to phenomena recently described for Huntington's disease neurons (28), characterized by the accumulation of the neurotoxic htt protein due to cargo recognition failure responsible for inefficient autophagy (28, 39).

To verify whether the increased numbers of empty AVs in cells coexposed to GX and FP reflect inefficient autophagy, a filter trap assay was performed to assess the efficiency of autophagy in removing intracellular protein aggregates (12, 36). Cotreatment with GX and FP strikingly increased the numbers of detergent-insoluble, ubiquitin-positive protein aggregates trapped on cellulose acetate filter membranes (Fig. 2B), consistent with a diminished clearance of cytosolic components via selective autophagy (22, 36). Moreover, both FP and another Cdk inhibitor, SCH727965 (dinaciclib) (40), also clearly increased the accumulation of polyubiquitinated proteins in GX-treated cells (Fig. 2C). Furthermore, immunofluorescence staining using an antiubiquitin antibody demonstrated that cotreatment with GX and FP resulted in a marked increase in the number of ubiquitin-positive protein aggregates (Fig. 2D). Interestingly, LysoTracker staining revealed that GX also dramatically increased lysosome mass and number (Fig. 2E), presumably reflecting enhanced lysosome biogenesis required for increased autophagy. Nevertheless, coadministration of FP increased neither lysosome mass or number in cells exposed to GX (Fig. 2E) nor expression levels of TFEB (see Fig. S1E in the supplemental material), a transcription factor critical for the coupling of autophagosome formation and lysosome bio-

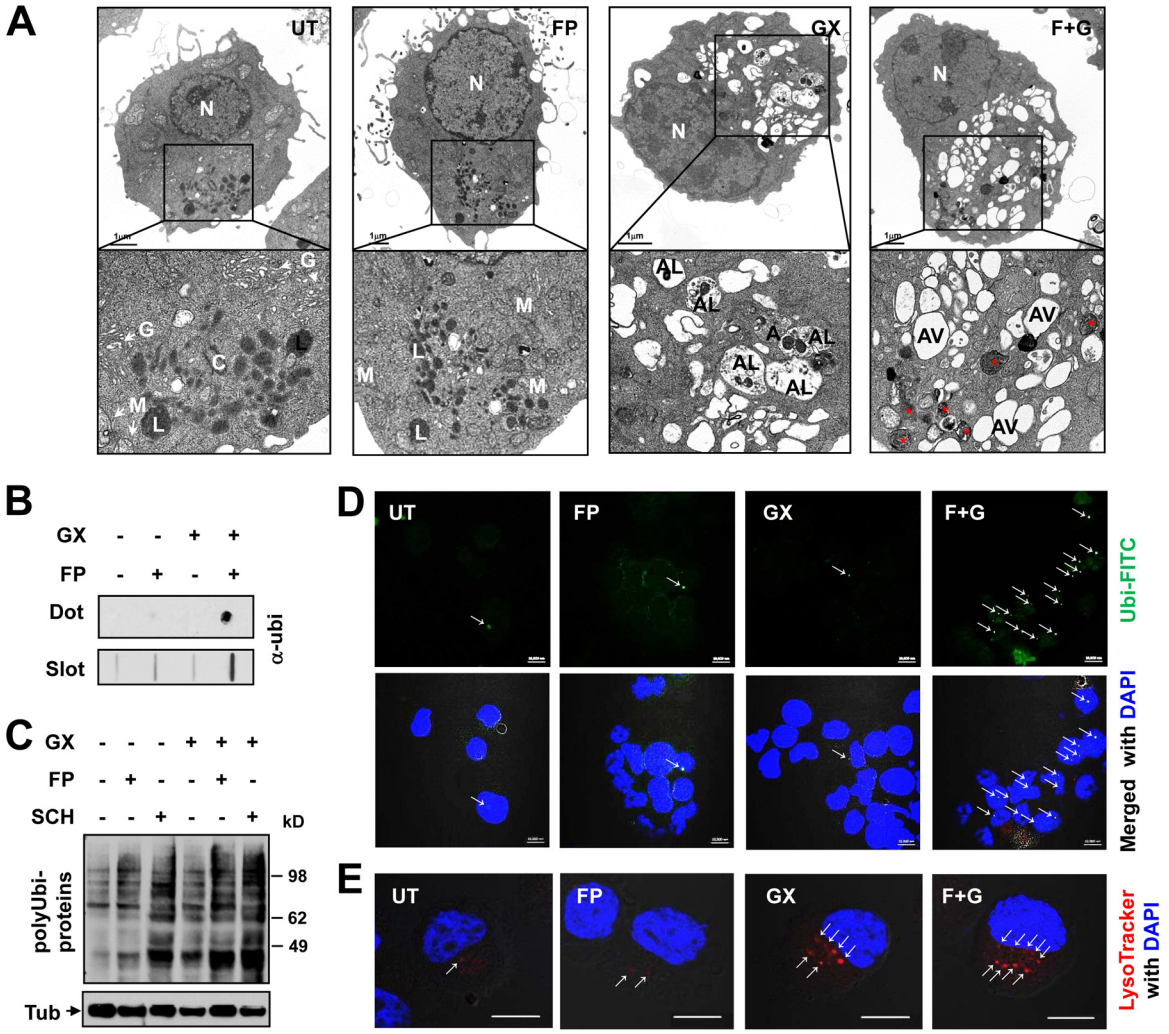

FIG 2 Cotreatment with BH3 mimetics and Cdk inhibitors results in inefficient autophagy. (A) U266 cells were exposed (16 h) to 500 nM GX with or without 100 nM FP and then examined by electron microscopy (bar = 1 μm). Asterisks indicate deformed mitochondria. N, nucleus; M, mitochondrion; L, lysosome; G, Golgi apparatus; C, centrosome; A, autophagosome; AL, autolysosome; AV, autophagic vacuoles with clear content (empty). (B) In parallel, a filter trap assay using dot or slot blots probed with an antiubiquitin antibody (α-ubi) was performed to monitor the intracellular accumulation of SDS-insoluble ubiquitin-positive protein aggregates. (C) U266 cells were treated (16 h) with 500 nM GX with or without 100 nM FP or 5 nM SCH727965, after which immunoblot analysis was performed to monitor the accumulation of polyubiquitinated (polyUbi) proteins using an antiubiquitin antibody. (D and E) Alternatively, cells were stained with antiubiquitin antibody (D) to monitor intracellular ubiquitin-positive protein aggregates (arrows) or with LysoTracker (E) to visualize lysosomes (arrows).

genesis (41). These results argue against the possibility that accumulation of AVs and ubiquitinated protein aggregates stems from a failure of autophagosome removal due to impaired lysosome biogenesis or autophagosome maturation, the disruption of which has been linked to cell death (42). Together, these findings indicate that coadministration of a Cdk inhibitor with an autophagy-inducing BH3 mimetic triggers inefficient autophagy characterized by an impaired ability of cells to clear ubiquitinated, malfolded proteins.

Cdk inhibition blocks SQSTM1/p62 expression during BH3 mimetic-induced autophagy. As the adaptor protein p62 plays a key role in recognition and loading of cargo during selective autophagy (20), the time course of p62 expression in cells exposed to GX with or without FP was monitored. Interestingly, protein levels of p62 varied at different intervals in untreated U266 cells (see Fig. S2A in the supplemental material), presumably reflecting basal and spontaneous autophagy, as observed in U266 cells expressing GFP-LC3 (Fig. 1A). GX triggered LC3 processing by as early as 6 h, accompanied by the induction of p62 (Fig. 3A; see also Fig. S2A in the supplemental material), as reported previously (38). Quantification of immunoblots after exposure to GX (e.g., 500 nM) revealed that whereas LC3-II expression persisted for 48 h (see Fig. S2B in the supplemental material), p62 levels fluctuated in a time-dependent manner over the entire exposure interval (Fig. 3B). As p62 itself undergoes autophagic degradation (23), the fluctuation of p62 levels reflects a dynamic balance between *de novo* synthesis and elimination via autophagy (43, 44). Notably, FP markedly attenuated p62 expression induced by GX (Fig. 3A and B). Similar events were also observed in other human MM cells or when the pan-Cdk inhibitor SCH727965 was employed (Fig. 3C; see also Fig. S2C in the supplemental material). Moreover, quantitative PCR demonstrated that FP significantly

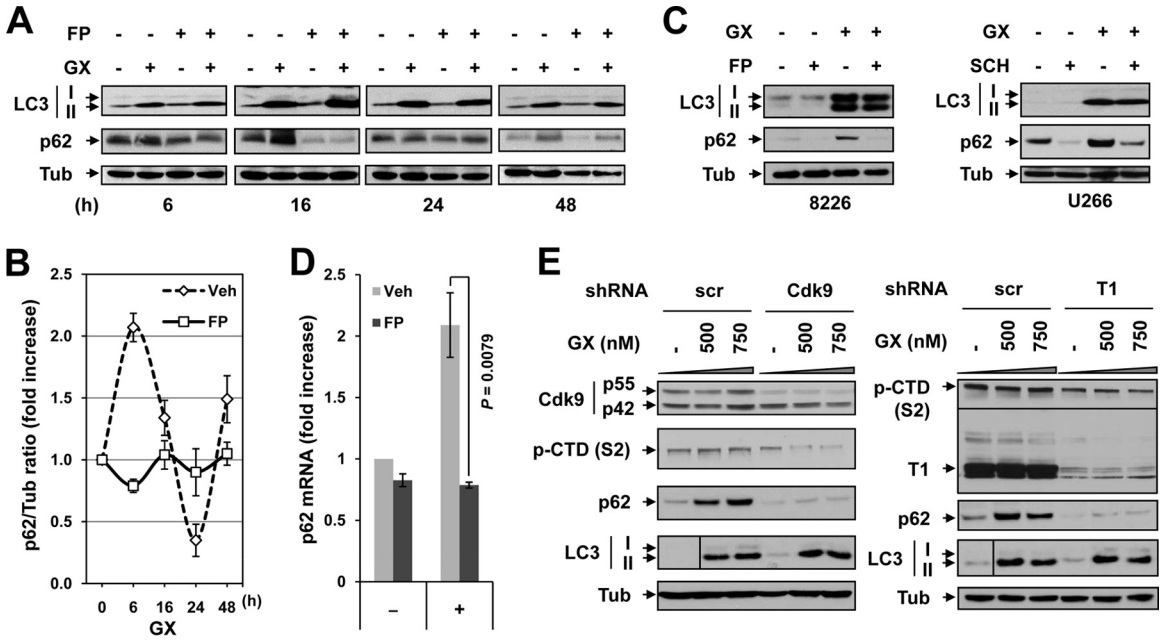

FIG 3 Cdk inhibition downregulates SQSTM1/p62 but fails to affect LC3 processing during autophagy. (A) U266 cells were treated with 500 nM GX with or without 100 nM FP for 6, 16, 24, and 48 h, after which immunoblot analysis was performed to monitor LC3 processing and p62 expression. (B) Blots of p62 were quantified relative to tubulin (Tub) values (fold increase over the vehicle-treated control) (results represent means ± SD for three experiments). (C) RPMI8226 and U266 cells were treated (16 h) with GX (500 nM) with or without FP (100 nM) or SCH727965 (5 nM), after which LC3-II and p62 levels were determined by immunoblot analysis. (D) U266 cells were treated (6 h) with 500 nM GX (as indicated on the *x* axis) with or without 100 nM FP, after which qPCR was used to monitor p62 mRNA levels (fold increase over the vehicle-treated control) (means ± SD for three experiments). (E) U266 cells were stably transfected with constructs encoding shRNA targeting Cdk9 (left) or its partner cyclin T1 (right), which form the P-TEFb complex, and a scrambled sequence (scr) as a negative control. The cells were then exposed (16 h) to GX, followed by immunoblot analysis to monitor the expression of Cdk9 (p42 and p55 isoforms) or cyclin T1, CTD phosphorylation (p-CTD) (serine 2) of RNA polymerase II, LC3 processing, and p62 expression. The vertical lines (LC3) indicate where additional sample lanes were removed from the images; the horizontal line (phosphorylated CTD and cyclin T1) indicates the splice site in the composite image derived from a single blot.

blocked GX-induced p62 expression at the transcriptional level (Fig. 3D). Furthermore, inhibition of protein synthesis by cycloheximide (CHX) also blocked p62 induction by GX (see Fig. S2D in the supplemental material). Together, these results indicate that FP inhibits *de novo* synthesis of p62 during autophagy.

To further determine whether Cdk inhibitors block p62 transcription due to inhibition of Cdk9, a key component of positive transcription elongation factor b (P-TEFb) (a complex of Cdk9 and its partner cyclin T1 [45]), Cdk9 or cyclin T1 was knocked down by using the respective shRNAs. Cdk9 or cyclin T1 knockdown sharply reduced C-terminal domain (CTD) phosphorylation of RNA polymerase II (Pol II) at serine 2 (Fig. 3E), an event specifically mediated by Cdk9 and required for mRNA elongation (45). Notably, GX failed to trigger p62 expression in these cells, while no effect on GX-induced LC3 processing was observed, consistent with results obtained by employing pharmacological Cdk inhibitors (Fig. 3A to C). These findings indicate that Cdk9 inhibition blocks p62 expression but does not prevent autophagy induction in GX-treated cells.

SQSTM1/p62 downregulation leads to cargo loading failure during autophagy in association with increased cell death. The functional role of p62 downregulation by Cdk9 inhibition in autophagy induced by GX was then examined. First, the effects of disrupting autophagy by pharmacological or genetic approaches on p62 expression were tested in cells coexposed to GX and FP. As anticipated, spautin-1, an inhibitor of the ubiquitin-specific peptidases USP10 and USP13, which target the beclin-1 subunit of Vps34 complexes (46), and 3-methyladenine (3-MA), which blocks autophagosome formation via inhibition of type III phosphatidylinositol 3-kinase (PI-3K) (47), clearly reduced LC3 processing in cells cotreated with GX and FP (Fig. 4A; see also Fig. S2E in the supplemental material). These events were accompanied by an accumulation of p62, consistent with evidence that p62 is turned over primarily through autophagy (22, 23). Significantly, GX-FP cotreatment dramatically downregulated p62 expression under these conditions (Fig. 4A; see also Fig. S2E in the supplemental material). Similar phenomena were observed when autophagy was genetically disrupted by shRNA at early stages (e.g., Ulk1 [Fig. 4B], which acts in the Atg1/Ulk complex essential for autophagy initiation [13]) or late stages (e.g., Lamp2 [see Fig. S2F in the supplemental material], a lysosome membrane protein essential for autophagosome maturation [13]) of autophagy.

Second, the effects of p62 on cargo loading were then examined by using a filter trap assay employing antibodies directed against p62 or ubiquitin. GX induced a marked increase in the amount of p62 bound to protein aggregates trapped on the membrane (see Fig. S2G, top, in the supplemental material), an event required for loading of cargo onto autophagosomes (17). Importantly, this process was substantially diminished by FP or SCH727965, accompanied by a marked intracellular accumulation of ubiquitin-positive protein aggregates (Fig. 2B and D) as well as by accumulation of polyubiquitinated proteins (Fig. 2C), collectively indicating autophagy dysfunction due to cargo loading failure. Moreover, accumulation of polyubiquitinated proteins (Fig. 4C) or ubiquitin-

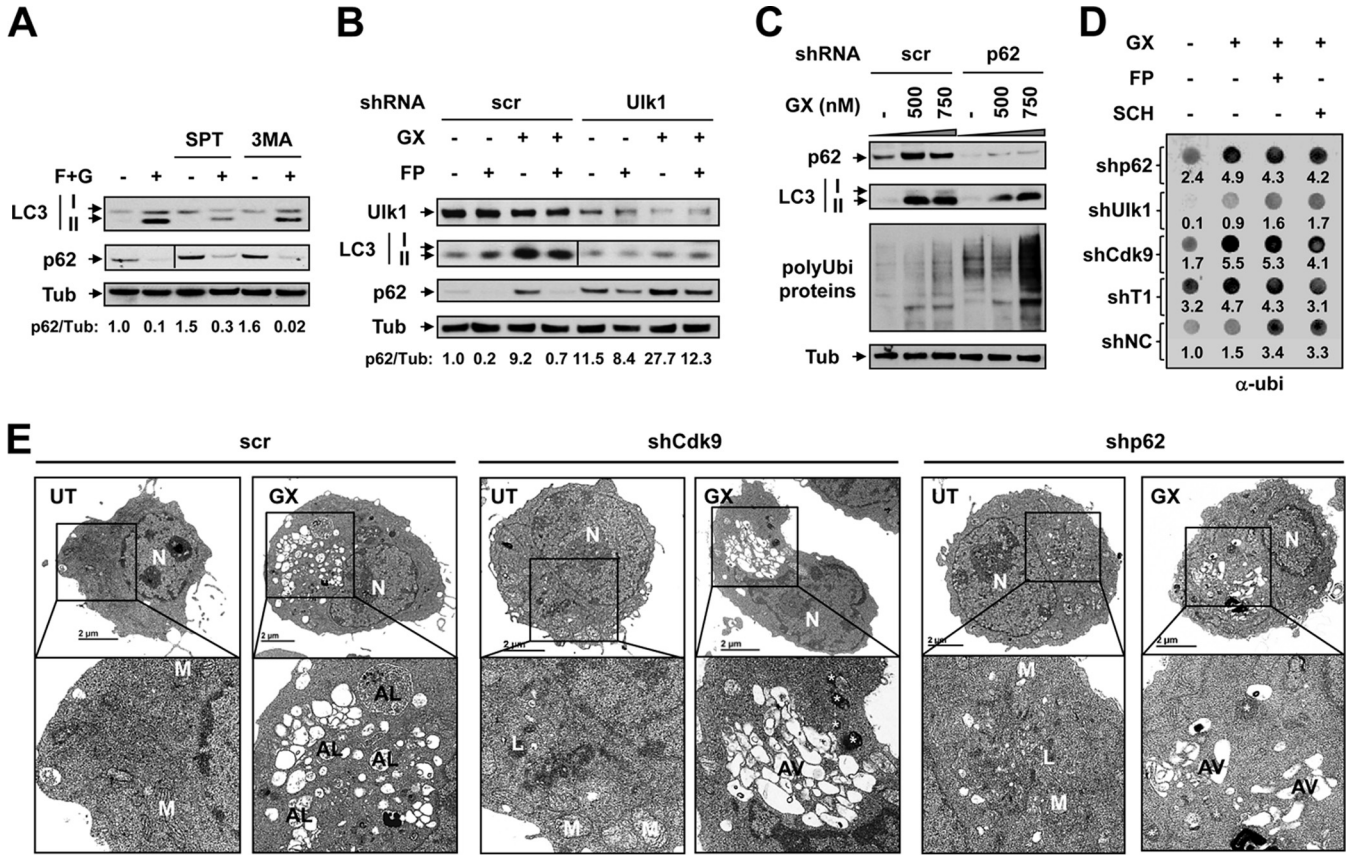

FIG 4 SQSTM1/p62 downregulation results in cargo loading failure and inefficient autophagy. (A) U266 cells were exposed (16 h) to 100 nM FP plus 500 nM GX in the presence or absence of 7.5 μM spautin-1 (SPT) or 500 μM 3-methyladenine (3-MA), after which LC3 processing and p62 expression were monitored by immunoblot analysis. The vertical line (p62) indicates where additional sample lanes were removed from the image. Values indicate quantification of p62 relative to values for tubulin (fold increase over the untreated control). (B) U266 cells were stably transfected with constructs encoding shRNA targeting Ulk1 or a scrambled sequence as a negative control. Cells were then exposed (16 h) to 500 nM GX with or without 100 nM FP, followed by immunoblot analysis using the indicated antibodies. The vertical line (LC3) indicates where additional sample lanes were removed from the image. Values indicate quantification of p62 relative to tubulin values (fold increase over the untreated control). (C) U266 cells were stably transfected with constructs encoding shRNA targeting p62 or a scrambled sequence and then treated (16 h) with the indicated concentrations of GX (nM), followed by immunoblot analysis for p62 expression, LC3 processing, and intracellular accumulation of polyubiquitinated proteins. (D) U266 cells stably transfected with shRNA directed against p62, Ulk1, Cdk9, cyclin T1, or the scrambled sequence as a control were exposed (16 h) to 500 nM GX in the presence or absence of 100 nM FP or 5 nM SCH727965, followed by a filter trap assay using an antiubiquitin antibody to monitor ubiquitin-positive protein aggregates. Values indicate quantification of the amount of total ubiquitin-positive proteins in SDS-insoluble aggregates (values represent fold increases over the untreated controls of shNC cells). (E) U266 cells stably transfected with shRNA directed against Cdk9, p62, or the scrambled sequence as a control were exposed (16 h) to 500 nM GX and examined by electron microscopy (bar = 2 μm).

positive protein aggregates (Fig. 4D) was also observed in GX-treated cells in which p62 was directly knocked down by shRNA, compared to the scrambled shRNA control, whereas GX-induced LC3 processing was modestly reduced. Similarly, accumulation of ubiquitin-positive protein aggregates was also observed in GX-treated cells transfected with shRNA against either Cdk9 (Fig. 4D) or its partner cyclin T1 (Fig. 4D) but not Ulk1 (Fig. 4D). However, in contrast to cells transfected with the scrambled shRNA control, coadministration of either FP or SCH727965 failed to further increase the accumulation of ubiquitin-positive protein aggregates in these cells (Fig. 4D), presumably because p62 upregulation was already blocked directly by p62 shRNA or indirectly via Cdk9 inhibition/downregulation (e.g., by Cdk9 or cyclin T1 shRNA).

Third, following exposure to GX for 16 h, p62 or Cdk9 knockdown cells were examined by electron microscopy (Fig. 4E). Consistent with observations in parental cells (Fig. 2A), GX induced a marked increase in the number of autophagosomes/autolysosomes containing identifiable cellular organelles in U266 cells transfected with the scrambled shRNA control. Notably, whereas p62 knockdown modestly reduced the number of AVs after GX treatment, most AVs exhibited clear content in cells transfected with either Cdk9 or p62 shRNA (Fig. 4E), analogous to cells coexposed to GX and FP (Fig. 2A). In contrast, knockdown of Cdk9 did not affect autophagic flux following GX treatment, manifested by equivalent increases in numbers of both autophagosomes (yellow, mCherry plus GFP) and autolysosomes (red, mCherry only) compared to the scramble shRNA controls (Fig. 5A). Notably, similar phenomena were also observed for p62 knockout (ko) MEFs (30), compared to wild-type (wt) MEFs (Fig. 5B).

Finally, transient expression of GFP-tagged p62 (30) but not GFP only significantly rescued cells from increased GX lethality in U266 cells transfected with p62 shRNA (Fig. 5C). Consistent with the increased GX sensitivity of p62 knockdown U266 cells, p62 ko MEFs were also significantly more sensitive to GX than wt MEFs

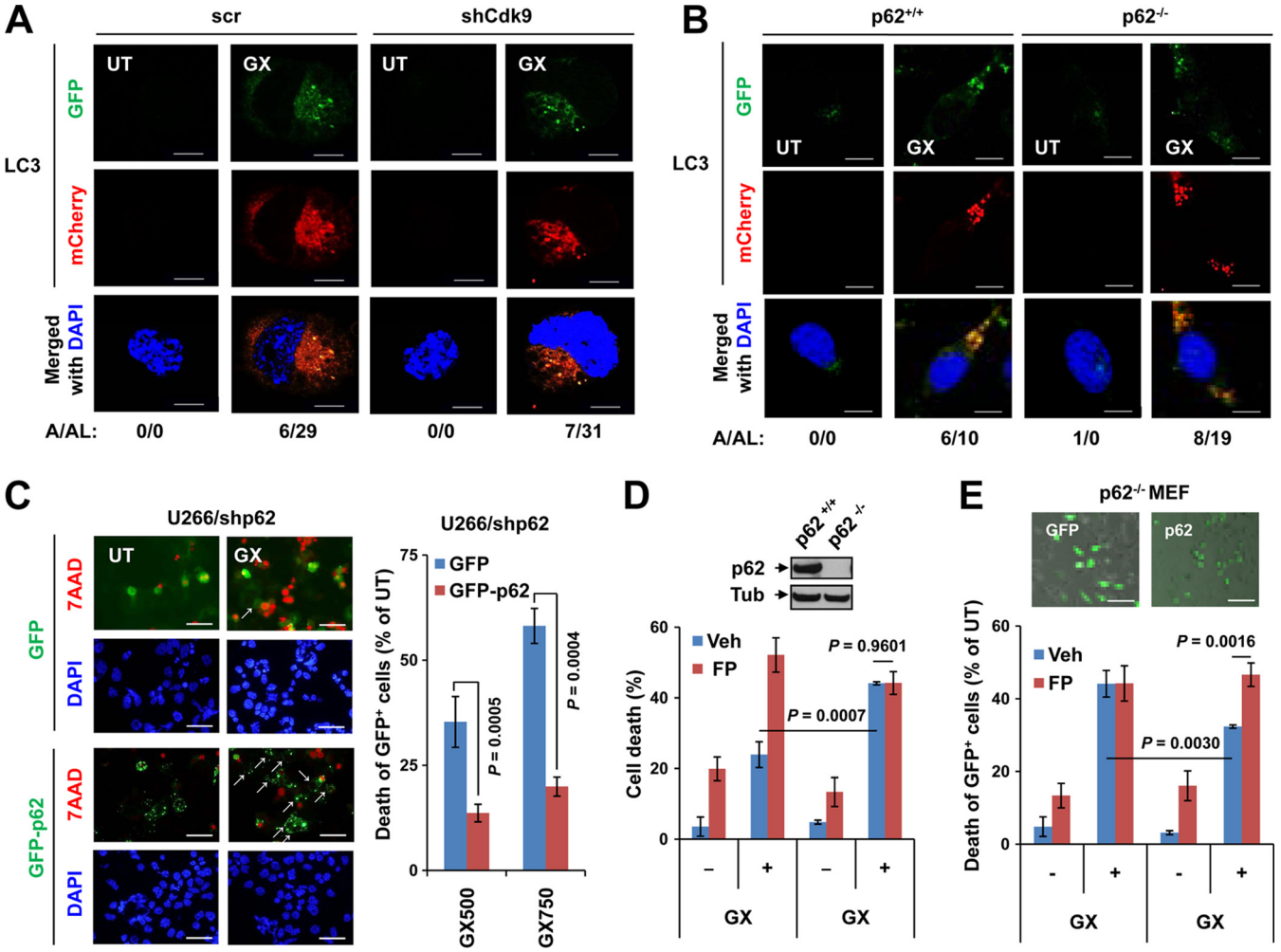

FIG 5 Expression of SQSTM1/p62 diminishes the increased lethality of BH3 mimetics in p62-defective cells. (A and B) U266 cells stably transfected with shRNA directed against Cdk9 or a scrambled sequence (A) or wild-type ($p62^{+/+}$) and p62 knockout ($p62^{-/-}$) MEFs (B) were transiently transfected with a pBABE-puro mCherry-EGFP-LC3B plasmid. After 6 h, cells were treated with GX (U266 cells, 500 nM; MEFs, 200 nM) for an additional 16 h, followed by analysis of autophagic flux using confocal microscopy (bar = 5 μm [A] or 10 μm [B]). Values indicate the number of autophagosomes (A) (yellow) and autolysosomes (AL) (red). (C) U266 cells stably transfected with p62 shRNA were transiently transfected with a construct encoding GFP-tagged p62 or GFP. After 6 h, cells were treated (24 h) with 500 nM GX, followed by 7-aminoactinomycin D (7AAD) staining to monitor cell death by confocal microscopy (left). Arrows indicate GFP-positive/7AAD-negative cells. Dead (7AAD-positive) cells in the GFP-positive population were then quantified by using flow cytometry (right). (D) Immunoblotting analysis was performed to validate p62 expression in wild-type and p62 ko MEFs (inset). MEFs (left, wt; right, p62 ko) were then exposed to 200 nM GX with or without 100 nM FP for 24 h, followed by 7AAD staining to determine the percentage of cell death by flow cytometry. (E) p62 ko MEFs were transiently transfected with GFP-tagged p62 or GFP (inset) (bar = 30 μm). After 6 h, cells were treated with 200 nM GX with or without 100 nM FP, after which the percentage of cell death was determined by flow cytometry (left, GFP; right, GFP-p62) as described above.

(Fig. 5D). Importantly, whereas FP strikingly potentiated GX lethality in wt MEFs, it failed to do so in p62 ko MEFs, presumably due to the inability of FP to downregulate p62 in p62 ko cells. Furthermore, transient expression of p62 significantly rescued p62 ko MEFs from enhanced GX lethality while at the same time partially restoring the ability of FP to potentiate GX-mediated cell death (Fig. 5E). Together, these findings argue that inhibition of p62 expression (e.g., by FP) during BH3 mimetic-induced autophagy results in an inefficient form of autophagy characterized by failure to load cargo (e.g., malfolded proteins) into autophagosomes, accompanied by significantly increased sensitivity to BH3 mimetics.

NBK/Bik is upregulated during inefficient autophagy. Bik, a BH3-only endoplasmic reticulum (ER)-associated proapoptotic protein (48), has recently been shown to promote autophagy by facilitating the release of beclin-1 from Bcl-2 (49). As a positive control, the proteasome inhibitor bortezomib clearly induced Bik upregulation (Fig. 6A), as previously described (50). Importantly, FP-GX coexposure robustly upregulated Bik (Fig. 6A), in association with sharply increased apoptosis (see Fig. S1C in the supplemental material). Similar events occurred in cells coexposed to GX and SCH727965 (Fig. 6B; see also Fig. S3A in the supplemental material). Notably, knockdown of either Cdk9 or cyclin T1 by shRNA recapitulated the effects of Cdk inhibitors on upregulating Bik and potentiating GX-induced apoptosis (Fig. 6C; see also Fig. S3B in the supplemental material).

To determine the subcellular localization of Bik, ER membrane fractions were separated and subjected to immunoblot probing

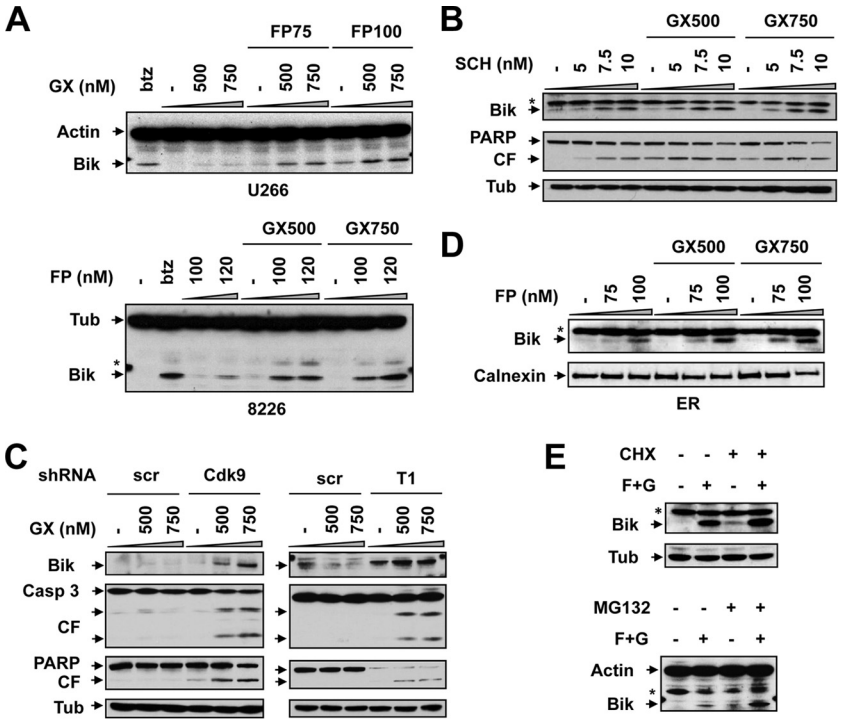

FIG 6 Cdk9 inhibition upregulates NBK/Bik in cells exposed to BH3 mimetics. (A and B) U266 and RPMI8226 cells were treated (24 h) with the indicated concentrations of GX with or without FP (A), SCH727965 (5 nM) (B), or bortezomib (btz) (4 nM) as a positive control, after which immunoblot analysis was performed to monitor Bik expression and/or PARP cleavage. *, nonspecific band. (C) U266 cells stably transfected with shRNA directed against Cdk9, cyclin T1, or a scrambled sequence as a control were exposed (24 h) to 500 nM or 750 nM GX, followed by immunoblot analysis to monitor the expression of Bik and cleavage of caspase 3 and PARP. (D) After U266 cells were treated (24 h) with the indicated concentrations of GX (nM) with or without FP (nM), the ER membrane fraction was isolated and subjected to immunoblot analysis to monitor the subcellular localization of Bik. The same membranes were probed by an anticalnexin antibody as a loading control for ER membranes. (E) U266 cells were treated (16 h) with 500 nM GX plus 100 nM FP in the presence or absence of 1 μM CHX (top) or 300 nM MG-132 (bottom), followed by immunoblot analysis to monitor Bik expression.

for Bik. As described previously (48), Bik localized primarily to the ER membrane (Fig. 6D), accompanied by mitochondrial translocation of Bax and release of mitochondrial proteins (e.g., cytochrome *c* and AIF) (see Fig. S3C in the supplemental material), but not to the mitochondria (see Fig. S3D in the supplemental material). In contrast, Bim, another BH3-only protein, localized predominantly to the mitochondria.

The mechanism(s) by which FP-GX upregulates Bik was then assessed. Inhibition of *de novo* protein synthesis by CHX failed to prevent Bik upregulation following FP-GX treatment (Fig. 6E, top), whereas quantitative PCR revealed the absence of significant changes in Bik mRNA levels following exposure of cells to FP and GX individually or in combination (see Fig. S3E in the supplemental material). Moreover, the proteasome inhibitor MG-132 (51) (Fig. 6E, bottom) or bortezomib (see Fig. S3F in the supplemental material) further increased FP-GX-induced Bik expression, suggesting that a protein turnover-related mechanism is responsible for Bik upregulation.

NBK/Bik accumulation stems from cargo loading failure. Because autophagic degradation represents a major mechanism regulating protein turnover, the contributions of autophagy to Bik upregulation were evaluated. First, time course and dose-response analyses revealed clearly discernible increases in Bik expression levels (Fig. 7A). Quantification of immunoblots following exposure of cells to GX with or without FP revealed that Bik upregulation was first discernible 16 h after FP-GX coexposure (Fig. 7B), an interval substantially longer than that for autophagy induction (e.g., LC3 processing) first noted at 6 h (see Fig. S2B in the supplemental material), which persisted over the ensuing 24 h. Interestingly, disruption of autophagy by spautin-1 or 3-MA, which blocks autophagy initiation (47), diminished Bik upregulation and reduced apoptosis (e.g., PARP cleavage) induced by FP-GX (Fig. 7C). Similar phenomena were observed for cells transfected with shRNA directed against Ulk1 (Fig. 7D), beclin-1, or Atg5 (Fig. 7E; see also Fig. S3G in the supplemental material), proteins critical for autophagy initiation (13). In sharp contrast, chloroquine (CQ), which blocks autophagy maturation (47), further enhanced Bik upregulation induced by FP-GX, accompanied by increased PARP cleavage (Fig. 7C). Analogous results were obtained with U266 cells stably transfected with p62 shRNA (see Fig. S3H in the supplemental material). Similarly, Lamp2 knockdown also promoted Bik accumulation and significantly sensitized cells to FP-GX (see Fig. S3I in the supplemental material). These findings suggest that Bik upregulation likely occurs during autophagy and primarily stems from disruption of the later stages of autophagy, particularly cargo loading into autophagosomes and/or subsequent events (e.g., lysosomal degradation through autophagosome maturation).

In addition, whereas ectopic expression of either Bcl-2 (see Fig. S4A in the supplemental material), Bcl-x_L (see Fig. S4B in the supplemental material), Mcl-1 (see Fig. S4C in the supplemental material), or dominant negative caspase 9 (see Fig. S4D in the

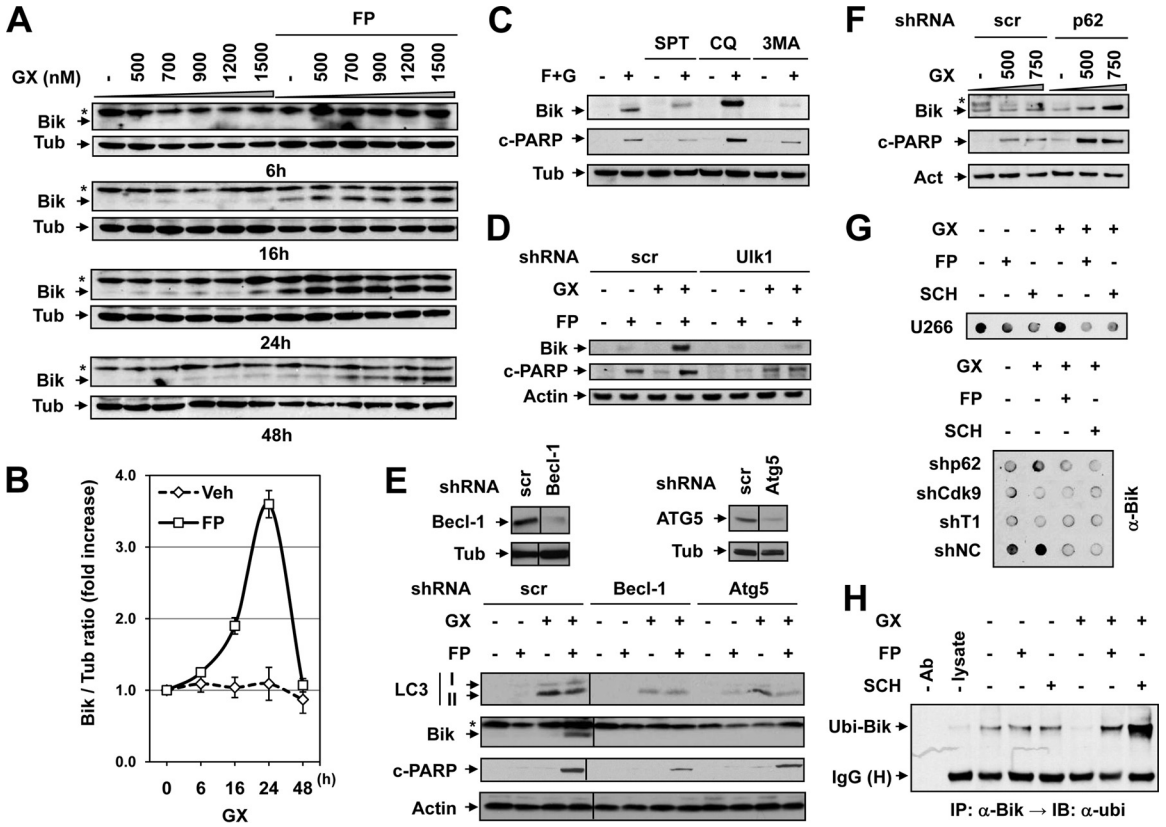

FIG 7 NBK/Bik upregulation occurs during autophagy in association with loading failure. (A) U266 cells were treated with the indicated concentrations of GX with or without FP (100 nM) for 6, 16, 24, and 48 h, after which Bik expression was monitored by immunoblot analysis. (B) Blots of Bik after treatment with 500 nM GX with or without FP were quantified relative to tubulin values (values represent fold increases over the vehicle-treated controls) (means ± SD for three experiments). (C) U266 cells were cotreated (24 h) with 500 nM GX and 100 nM FP in the presence or absence of 7.5 μM spautin-1 (SPT), 50 μM CQ, or 500 μM 3-MA. After treatment, Bik expression and PARP cleavage were determined by immunoblot analysis. (D and E) U266 cells stably transfected with shRNA directed against Ulk1 (D), beclin-1 and Atg5 (E), or the scrambled sequence as a control were exposed (24 h) to 500 nM GX with or without 100 nM FP, followed by immunoblot analysis to monitor Bik expression and PARP cleavage. Vertical lines indicate where additional sample lanes were removed from the images. (F) U266 cells stably transfected with shRNA of p62 or the scrambled sequence as a control were exposed (24 h) to 500 or 750 nM GX, followed by immunoblot analysis for Bik expression and PARP cleavage. (G) U266 cells were exposed (16 h) to 500 nM GX with or without 100 nM FP or 5 nM SCH727965 (top), and U266 cells stably transfected with shRNA directed against p62, Cdk9, cyclin T1, or the scrambled sequence as a control were treated (16 h) with 500 nM GX with or without 100 nM FP or 5 nM SCH727965 (bottom). After drug treatment, a filter trap assay using anti-Bik antibody (α-Bik) was performed to monitor the amount of Bik in SDS-insoluble protein aggregates. (H) U266 cells were exposed (16 h) to 500 nM GX with or without 100 nM FP or 5 nM SCH727965, followed by immunoprecipitation (IP) using anti-Bik antibody and subsequent immunoblot (IB) analysis using antiubiquitin antibody (α-ubi). Immunoprecipitations without anti-Bik antibody (− Ab) (lane 1) or cell lysate (− lysate) (lane 2) were used as controls. IgG(H), IgG heavy chain.

supplemental material) clearly blocked apoptosis induced by FP-GX, only Bcl-2 or Bcl-x_L attenuated autophagy induction (e.g., LC3 processing), presumably due to the sequestration of beclin-1 (4, 7), in association with the prevention of Bik upregulation. In sharp contrast, Mcl-1 or dominant negative caspase 9 failed to diminish autophagy or block Bik upregulation. These observations further support the notion that initiation of autophagy, but not apoptosis, is required for Bik upregulation in cells coexposed to FP and GX.

It is noteworthy that p62 downregulation by FP occurred at 6 h (Fig. 3B), clearly prior to Bik upregulation (16 h) (Fig. 7B). Consequently, the relationship between p62 downregulation and Bik accumulation was then examined. Significantly, similarly to cells transfected with Cdk9 or cyclin T1 shRNA (Fig. 6C), knockdown of p62 also substantially increased Bik upregulation after GX treatment, accompanied by a markedly increased sensitivity of cells to GX (Fig. 7F; see also Fig. S4E in the supplemental material). In accordance with these findings, a filter trap assay probed with an anti-Bik antibody revealed that FP or SCH727965 substantially reduced the amount of Bik detected in protein aggregates (Fig. 7G, top). Consistent with these findings, shRNA against either p62, Cdk9, or cyclin T1 also substantially reduced the amount of Bik in protein aggregates, compared to the scrambled shRNA control, after GX treatment (Fig. 7G, bottom). Finally, coadministration of either FP or SCH727965 with GX led to a clear accumulation of ubiquitinated Bik in cells (Fig. 7H). Together, these findings argue that p62 downregulation disables the loading of Bik into protein aggregates and subsequently autophagosomes, thereby preventing its degradation via autophagy. Consequently, these findings raise the possibility that Bik upregulation stems from cargo loading failure and inefficient autophagy due to p62 downregulation.

NBK/Bik switches inefficient autophagy to apoptosis. Bik plays dual roles in the regulation of both apoptosis (48) and autophagy (49). The functional roles of Bik in this setting were then examined by using cells stably transfected with Bik shRNA. In these cells, FP-GX failed to upregulate Bik (Fig. 8A [bortezomib

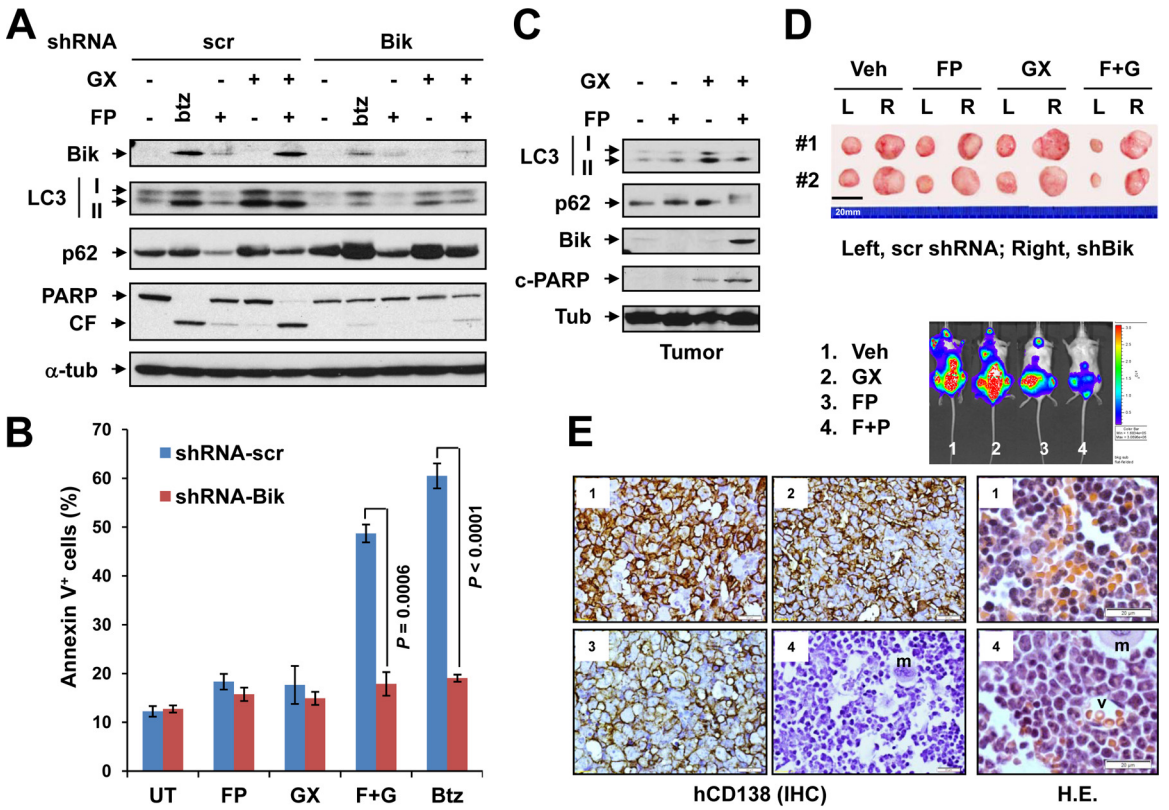

FIG 8 NBK/Bik plays a functional role in triggering apoptosis *in vitro* and *in vivo*. (A and B) U266 cells were stably transfected with a construct encoding shRNA directed against Bik or a scrambled sequence as a control and then treated (24 h) with 500 nM GX with or without 100 nM FP or 4 nM bortezomib (btz) as a positive control. Immunoblot analysis (A) and flow cytometry (B) were conducted to monitor the expression of the indicated proteins or to determine percentage of apoptotic (annexin V-positive) cells (values represent means ± SD for three experiments). (C) Athymic NCr-nu/nu mice subcutaneously inoculated in the flank with 5×10^6 RPMI8226 cells were treated with GX (3 mg/kg of body weight intramuscularly) with or without FP (5 mg/kg i.p.). Tumors were excised at day 28 after tumor cell inoculation and then homogenized and subjected to immunoblot analysis using the indicated antibodies. (D) NOD/SCID/gamma (NSG) mice were subcutaneously inoculated in each flank with 1×10^7 U266 cells stably transfected with shRNA directed against Bik (right flank) or a scrambled sequence as a control (left flank). FP (3 mg/kg i.p.) with or without GX (3 mg/kg i.p.) was then administered daily for a total of 11 days. Images of tumors removed from two representative mice were captured at day 49 after tumor cell inoculation (bar = 20 mm). (E) NSG mice were injected i.v. via the tail vein with 5×10^6 U266 cells carrying luciferase, after which FP (3 mg/kg i.p.) with or without GX (3 mg/kg i.p.) was administered daily for a total of 19 days. The bioluminescent images of representative mice were captured at day 35 after inoculation of cells. Lumbar vertebrae removed from mice were immunohistochemically (IHC) stained with anti-human CD138 antibody (bar = 10 μm) or hematoxylin and eosin (H.E.) (bar = 20 μm). m, megakaryocyte; v, blood vessel.

treatment is shown as a positive control]). Bik knockdown partially but discernibly reduced LC3 processing following exposure to GX with or without FP, consistent with evidence that Bik contributes to autophagy induction (49). In contrast, knockdown of another BH3-only protein, Bim, failed to attenuate GX-FP-induced autophagy (e.g., LC3 processing), although it substantially blocked apoptosis (see Fig. S4F in the supplemental material). Autophagy inhibition by Bik shRNA clearly increased p62 levels (Fig. 8A), presumably due to an inhibition of autophagy initiation (49). Importantly, the prevention of Bik upregulation sharply diminished apoptosis, reflected by the virtually complete abrogation of PARP cleavage (Fig. 8A) and annexin V positivity (Fig. 8B) induced by FP-GX as well as by bortezomib (50). However, while EM analysis confirmed marked reductions in the number and size of AVs in Bik shRNA cells exposed to GX, Bik knockdown did not prevent the formation of empty AVs following FP-GX cotreatment (see Fig. S5 in the supplemental material).

Of note, administration of GX induced LC3 processing and p62 expression in tumor samples excised from a xenograft RPMI8226 flank model. Significantly, FP coadministration diminished GX-mediated p62 upregulation, accompanied by clear increases in levels of Bik expression and PARP cleavage *in vivo* (Fig. 8C). Furthermore, in a dual-sided flank mouse model, tumors generated from Bik shRNA cells (right flank) displayed pronounced resistance to combined treatment with FP and GX compared to those derived from scrambled-sequence shRNA cells (left flank) (Fig. 8D). Finally, in a tail vein intravenous (i.v.) orthotopic mouse model, coadministration of FP and GX substantially reduced tumor burden, reflected by low luciferase signals (Fig. 8E, top), and strikingly eliminated human CD138-positive tumor cells (bottom) while restoring normal bone marrow structure (bottom right). Together, these findings argue strongly that Bik upregulation plays an important functional role in converting inefficient autophagy to apoptosis.

DISCUSSION

Apoptosis (type I) and autophagy (type II) represent the two major forms of programmed cell death. Importantly, these processes share common molecular pathways regulated by Bcl-2 family proteins (3, 4) and often occur in concert, e.g., following exposure to

agents, such as BH3 mimetics (i.e., GX-015-070 [obatoclax] and ABT-737), that target Bcl-2 family proteins (e.g., Bcl-2 and Bcl-xL) (8). While apoptosis represents an important prodeath mechanism through which chemotherapeutic agents and ionizing radiation induce tumor cell demise, autophagy generally functions as a prosurvival mechanism by maintaining cellular homeostasis and metabolism (2, 14), thus conferring resistance to various types of therapy (2, 52). While the optimal autophagy-targeting strategy remains the subject of debate (9, 10), improving the efficacy of and circumventing resistance to anticancer drugs by converting a cytoprotective autophagic response to apoptosis would represent an attractive approach, e.g., by targeting cross talk between these processes. For example, multiple autophagy-related proteins, such as beclin-1 (53–55), Atg5 (56), and Atg4D (or LC3) (57), are substrates for caspases or calpains activated during apoptosis, while their cleaved fragments sensitize cells to apoptosis. Consequently, this form of cross talk generally represents a mechanism of apoptosis amplification through modification of autophagy-regulatory proteins. The findings described here highlight a novel mechanism underlying cross talk between autophagy and apoptosis and suggest that the adaptor protein SQSTM1/p62 and the BH3-only protein NBK/Bik represent key switches governing the critical decision of cells undergoing autophagy to survive or die. Specifically, these observations argue that targeting SQSTM1/p62 results in an inefficient form of autophagy due to cargo loading failure, leading to upregulation of the proapoptotic BH3-only protein NBK/Bik, which in turn triggers activation of the intrinsic apoptotic pathway.

The concept of inefficient autophagy was initially described for Huntington's disease (28), a genetic neurodegenerative disorder caused by an expanded polyglutamine tract in the huntingtin (htt) protein (58). In Huntington's disease neurons, autophagic vacuoles form at normal or increased rates but fail to recognize and trap cytosolic cargo in their lumen. Inefficient engulfment of cytosolic components by autophagosomes leads to slow turnover, functional decay, and accumulation of mutant htt within Huntington's disease cells (28, 39), which is noxious to neurons (22). Thus, whereas autophagy protects neurons (58), inefficient autophagy has been identified as a primary defect in Huntington's disease (28). Notably, in the present study, similar phenomena were observed for neoplastic cells exposed to autophagy inducers (e.g., BH3 mimetics) under conditions in which the adaptor protein p62 was transcriptionally downregulated through Cdk9 inhibition, e.g., by pharmacological Cdk inhibitors or shRNA directed against Cdk9 or cyclin T. Features of inefficient autophagy due to cargo loading failure in this setting resemble those previously described in the case of Huntington's disease, including (i) normal autophagic flux induced by GX in the presence or absence of Cdk inhibition, (ii) no discernible change in lysosome biogenesis in cells exposed to GX with or without Cdk inhibition, (iii) EM morphological demonstration of increased numbers of double-membraned autophagic vacuoles (AVs) with clear or empty contents following GX exposure in cells in which p62 was downregulated, (iv) functional evidence from filter trap assays demonstrating impaired autophagic removal of SDS-insoluble ubiquitinated protein aggregates (22, 36) when p62 was downregulated, and (v) the resulting accumulation of polyubiquitinated proteins in cells exposed to GX with FP or when p62 was knocked down by shRNA (22, 36).

The evidence described above suggests that the adaptor protein SQSTM1/p62, which is responsible for the loading of malfolded or unwanted proteins into autophagosomes for lysosomal degradation (21), serves as a switch that converts autophagy to an inefficient form. Consistent with the notion that SQSTM1/p62 acts to recognize and load cargo into autophagosomes for degradation, levels of this protein underwent dynamic changes during GX-induced autophagy, presumably reflecting the net effects of *de novo* synthesis versus autophagic degradation (23). Interestingly, prevention of autophagy at either the initiation phase (e.g., by shUlk1 [13], 3-MA [47], or spautin-1 [46]) or the maturation stage (e.g., by Lamp2 shRNA [13]) resulted in p62 accumulation. This suggests that p62 levels are regulated primarily via autophagic degradation (38). Importantly, knockdown of p62 by shRNA led to cargo loading failure-associated inefficient autophagy in a manner indistinguishable from that induced by genetic disruption or pharmacological inhibition of the P-TEFb (i.e., Cdk9/cyclin T) complex (45). In this context, inhibition of RNA Pol II (e.g., by Cdk9 inhibitors) diminishes the expression levels of various proteins with short half-lives (5), raising the possibility that a similar mechanism is operative in the case of downregulation of p62, a protein characterized by rapid turnover (23). Interestingly, p62 exerts a cytoprotective effect with respect to htt-induced cell death in Huntington's disease (22). However, evidence of a direct contribution of the p62-mediated cargo loading process to cytoprotective autophagy in neoplastic cells is currently lacking. The robust induction of apoptosis in BH3 mimetic-exposed cells when *de novo* p62 expression was blocked (e.g., by either Cdk9 inhibition or p62 shRNA) indicates that whereas p62 downregulation by itself is insufficient to trigger cell death, it may sensitize tumor cells to autophagy inducers such as GX by disabling the cargo loading process, resulting in inefficient autophagy. Finally, p62 has been reported to contribute to tumorigenesis either directly (26) or indirectly through NF-κB stimulation unrelated to its function in autophagy (59). Collectively, these observations argue that p62 represents a rational candidate target in cancer treatment. However, inasmuch as Cdk inhibitors (e.g., FP) inhibit global transcription, the possibility that other proteins implicated in autophagy regulation (particularly, e.g., cargo recognition/loading and autophagy maturation) also contribute to autophagy dysfunction in this setting cannot be excluded.

These findings identify NBK/Bik as a key molecule that converts inefficient autophagy to apoptosis. NBK/Bik exerts dual functions in regulating both autophagy and apoptosis (60). For example, Bik cooperates with NAF-1 to induce autophagy by releasing beclin-1 from Bcl-2 at the ER (49). However, in addition to its role as a regulator of autophagy and apoptosis, the disposition of Bik appears to be reciprocally governed by the former process. In support of this concept, the absence of changes in Bik mRNA and the failure of CHX to block Bik upregulation argue that increases in Bik protein levels involve posttranslational events. Indeed, inhibition of the two major mechanisms (i.e., proteasomal and autophagic degradation) responsible for the removal of ubiquitinated proteins (61) resulted in marked Bik accumulation. These findings argue that Bik may be a substrate for ubiquitination and degradation (51) through both the proteasomal and autophagic systems (61). Consistent with this notion, concomitant inhibition of proteasome function (e.g., by MG-132 or bortezomib) and autophagic degradation (e.g., by inefficient autophagy induced by GX in the setting of p62 downregulation) led

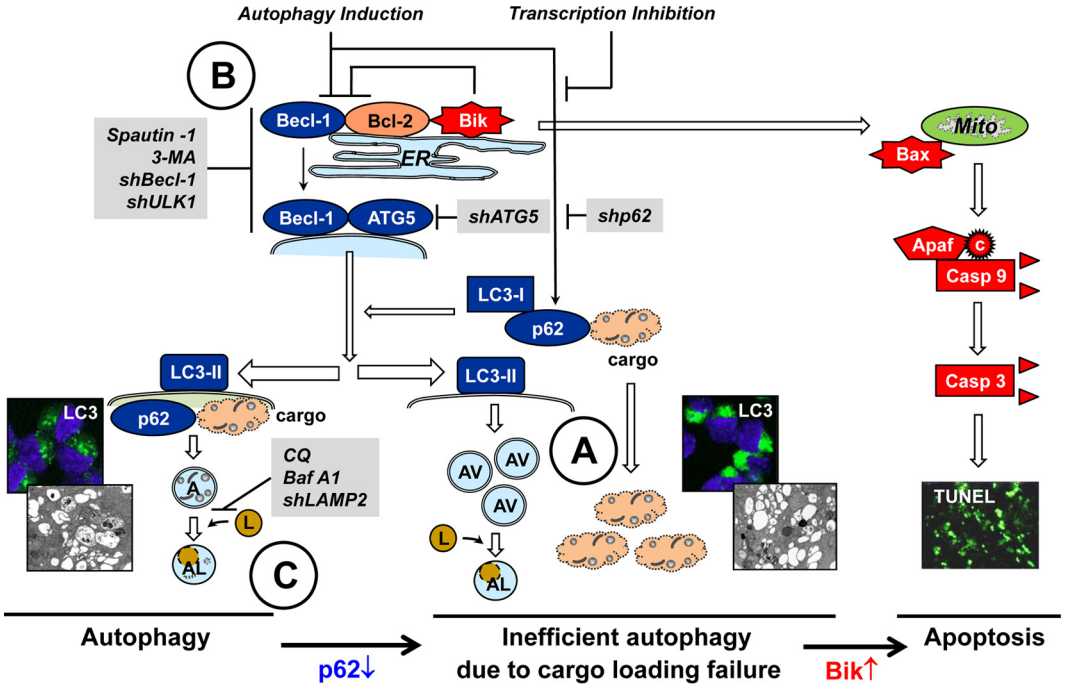

FIG 9 Mechanistic model of SQSTM1/p62 and NBK/Bik acting as novel molecular switches converting autophagy to apoptosis. During autophagy (e.g., induced by BH3 mimetics), the adaptor protein SQSTM1/p62 is responsible for recognition and loading of cargo, including malfolded (unfolded or misfolded) proteins and damaged organelles, into autophagosomes for removal. Targeting p62 by blocking its resynthesis through inhibition of transcription (e.g., by Cdk9 inhibition) disrupts this process, resulting in a failure of the cargo loading process and dysfunctional removal of malfolded proteins and damaged organelles, defined here as inefficient autophagy. The latter event promotes the accumulation of the BH3-only protein NBK/Bik, a substrate of ubiquitination and degradation via autophagy, which in turn triggers the activation of the apoptotic signaling cascade. Therefore, whereas targeting p62 converts cytoprotective autophagy into an inefficient form, NBK/Bik switches inefficient autophagy to apoptosis. Thus, SQSTM1/p62 and NBK/Bik cooperate to convert autophagy to apoptosis. This autophagy-targeting strategy (A) may provide theoretical advantages over alternatives, e.g., inhibition of autophagy initiation (B) or disruption of autophagosome maturation/fusion with lysosomes (C), including (i) upregulation of prodeath Bik, which requires autophagy initiation and does not occur in the case of stage B, and (ii) downregulation of oncogenic and prosurvival p62 at the transcriptional level by Cdk9 inhibition, in contrast to disruption of autophagy at either early (B) (e.g., initiation) or late (C) (e.g., maturation or lysosome biogenesis) stages, which results in p62 upregulation due to interference with its autophagic degradation. L, lysosome; c, cytochrome *c*.

to further increases in Bik accumulation compared to the inhibition of either arm individually. Interestingly, Bik accumulation appeared to be linked to autophagy, as inhibition of autophagy at the initiation stage (e.g., by beclin-1 [4, 6, 7], Ulk1, or Atg5 [13] shRNA; 3-MA [47]; or spautin-1 [46]) significantly diminished Bik upregulation and apoptosis. In this context, it has been reported that suppression of autophagy initiation attenuates cell death associated with impaired removal of autophagosomes (62). In contrast, dysfunction of later stages of autophagy (e.g., by CQ [47] or Lamp2 shRNA [13]) led to marked Bik accumulation and apoptosis induced by GX plus FP. Furthermore, these findings suggest that Bik accumulation stems from cargo loading failure secondary to p62 downregulation (e.g., by Cdk9 inhibition or p62 shRNA), evidenced by a reduction in the amount of Bik harbored by SDS-insoluble protein aggregates and the marked accumulation of ubiquitinated Bik (51). Finally, the dual roles of Bik are highlighted by the observations that knockdown of Bik by shRNA substantially reduced autophagy induced by GX and prevented apoptosis triggered by cotreatment with GX and FP both *in vitro* and *in vivo*.

In summary, a theoretical model, illustrated in Fig. 9, proposes a dynamic process in which targeting SQSTM1/p62 (e.g., via transcriptional repression by pharmacological or genetic Cdk9 inhibition) results in inefficient autophagy due to a failure of cargo loading, leading to the upregulation of Bik, which in turn triggers apoptosis. According to this model, SQSTM1/p62 and NBK/Bik represent two distinct but interconnected switches that convert cytoprotective autophagy to an inefficient form and subsequently to cell death. A corollary of these findings is that modulating such cross talk between autophagy and apoptosis via the SQSTM1/p62-NBK/Bik signaling axis could provide a novel avenue for therapeutic intervention. However, direct approaches to disrupt the function of adaptor proteins such as p62 are currently not available; instead, interfering with p62 expression at the transcriptional level might represent an attractive alternative, as many Cdk inhibitors, including those undergoing clinical evaluation (e.g., FP and SCH727965 [dinaciclib] [40]), exhibit potent inhibitory activity toward Cdk9 (45). Moreover, because p62 may exert multiple oncogenic functions, including those unrelated to its role in autophagy (e.g., NF-κB activation [59]), transcriptional downregulation of p62 offers the theoretical advantage of circumventing p62 accumulation resulting from the direct disruption of autophagy, e.g., by agents such as CQ (2, 52). Finally, there is the possibility that targeting p62 (e.g., by Cdk9 inhibitors) to induce apoptosis via NBK/Bik accumulation due to inefficient autophagy enhances the anticancer activity of

agents that, like BH3 mimetics, elicit a cytoprotective autophagic response.

ACKNOWLEDGMENTS

Wild-type and p62 gene knockout mouse embryonic fibroblasts as well as the pEGFP-p62 plasmid were gifts from Jorge Moscat (Sanford-Burnham Medical Research Institute). We thank Karla Kirkegaard (Stanford University) for the pEGFP-LC3 plasmid and Eric J. Brown (Genentech) for the pBABE-puro-mCherry-EGFP-LC3B plasmid.

This work was supported by awards P50 CA142509 to Y.D., S.C., R.Z.O., and S.G. and awards CA100866, CA93738, and CA167708 to S.G. and Y.D. from the National Institutes of Health; an award to S.G. from the Multiple Myeloma Research Foundation; and award R6238 to S.G. and Y.D. from the Leukemia and Lymphoma Society of America. Plasmid preparation was performed at the VCU Macromolecule Core Facility, supported in part by funding from NIH-NCI Cancer Center Core grant 5P30CA016059-29. Confocal microscopy and EM were performed at the VCU Department of Anatomy and Neurobiology Microscopy Facility, supported in part by funding from NIH-NINDS Center Core grant 5P30NS047463.

REFERENCES

1. **Elgendy M, Sheridan C, Brumatti G, Martin SJ.** 2011. Oncogenic Ras-induced expression of Noxa and Beclin-1 promotes autophagic cell death and limits clonogenic survival. Mol. Cell **42:**23–35. http://dx.doi.org/10.1016/j.molcel.2011.02.009.
2. **Janku F, McConkey DJ, Hong DS, Kurzrock R.** 2011. Autophagy as a target for anticancer therapy. Nat. Rev. Clin. Oncol. **8:**528–539. http://dx.doi.org/10.1038/nrclinonc.2011.71.
3. **Levine B, Sinha S, Kroemer G.** 2008. Bcl-2 family members: dual regulators of apoptosis and autophagy. Autophagy **4:**600–606.
4. **Pattingre S, Tassa A, Qu X, Garuti R, Liang XH, Mizushima N, Packer M, Schneider MD, Levine B.** 2005. Bcl-2 antiapoptotic proteins inhibit Beclin 1-dependent autophagy. Cell **122:**927–939. http://dx.doi.org/10.1016/j.cell.2005.07.002.
5. **Chen S, Dai Y, Pei XY, Myers J, Wang L, Kramer LB, Garnett M, Schwartz DM, Su F, Simmons GL, Richey JD, Larsen DG, Dent P, Orlowski RZ, Grant S.** 2012. CDK inhibitors up-regulate BH3-only proteins to sensitize human myeloma cells to BH3 mimetic therapies. Cancer Res. **72:**4225–4237. http://dx.doi.org/10.1158/0008-5472.CAN-12-1118.
6. **Liang XH, Jackson S, Seaman M, Brown K, Kempkes B, Hibshoosh H, Levine B.** 1999. Induction of autophagy and inhibition of tumorigenesis by beclin 1. Nature **402:**672–676. http://dx.doi.org/10.1038/45257.
7. **Maiuri MC, Le Toumelin G, Criollo A, Rain JC, Gautier F, Juin P, Tasdemir E, Pierron G, Troulinaki K, Tavernarakis N, Hickman JA, Geneste O, Kroemer G.** 2007. Functional and physical interaction between Bcl-X(L) and a BH3-like domain in Beclin-1. EMBO J. **26:**2527–2539. http://dx.doi.org/10.1038/sj.emboj.7601689.
8. **Bonapace L, Bornhauser BC, Schmitz M, Cario G, Ziegler U, Niggli FK, Schafer BW, Schrappe M, Stanulla M, Bourquin JP.** 2010. Induction of autophagy-dependent necroptosis is required for childhood acute lymphoblastic leukemia cells to overcome glucocorticoid resistance. J. Clin. Invest. **120:**1310–1323. http://dx.doi.org/10.1172/JCI39987.
9. **White E.** 2012. Deconvoluting the context-dependent role for autophagy in cancer. Nat. Rev. Cancer **12:**401–410. http://dx.doi.org/10.1038/nrc3262.
10. **White E, Dipaola RS.** 2009. The double-edged sword of autophagy modulation in cancer. Clin. Cancer Res. **15:**5308–5316. http://dx.doi.org/10.1158/1078-0432.CCR-07-5023.
11. **Amaravadi RK, Lippincott-Schwartz J, Yin XM, Weiss WA, Takebe N, Timmer W, Dipaola RS, Lotze MT, White E.** 2011. Principles and current strategies for targeting autophagy for cancer treatment. Clin. Cancer Res. **17:**654–666. http://dx.doi.org/10.1158/1078-0432.CCR-10-2634.
12. **Lee JY, Koga H, Kawaguchi Y, Tang W, Wong E, Gao YS, Pandey UB, Kaushik S, Tresse E, Lu J, Taylor JP, Cuervo AM, Yao TP.** 2010. HDAC6 controls autophagosome maturation essential for ubiquitin-selective quality-control autophagy. EMBO J. **29:**969–980. http://dx.doi.org/10.1038/emboj.2009.405.
13. **He C, Klionsky DJ.** 2009. Regulation mechanisms and signaling pathways of autophagy. Annu. Rev. Genet. **43:**67–93. http://dx.doi.org/10.1146/annurev-genet-102808-114910.
14. **Deretic V.** 2010. A master conductor for aggregate clearance by autophagy. Dev. Cell **18:**694–696. http://dx.doi.org/10.1016/j.devcel.2010.04.009.
15. **Dikic I, Johansen T, Kirkin V.** 2010. Selective autophagy in cancer development and therapy. Cancer Res. **70:**3431–3434. http://dx.doi.org/10.1158/0008-5472.CAN-09-4027.
16. **Kraft C, Peter M, Hofmann K.** 2010. Selective autophagy: ubiquitin-mediated recognition and beyond. Nat. Cell Biol. **12:**836–841. http://dx.doi.org/10.1038/ncb0910-836.
17. **Itakura E, Mizushima N.** 2011. p62 targeting to the autophagosome formation site requires self-oligomerization but not LC3 binding. J. Cell Biol. **192:**17–27. http://dx.doi.org/10.1083/jcb.201009067.
18. **Weidberg H, Shvets E, Elazar Z.** 2011. Biogenesis and cargo selectivity of autophagosomes. Annu. Rev. Biochem. **80:**125–156. http://dx.doi.org/10.1146/annurev-biochem-052709-094552.
19. **Kirkin V, Lamark T, Sou YS, Bjorkoy G, Nunn JL, Bruun JA, Shvets E, McEwan DG, Clausen TH, Wild P, Bilusic I, Theurillat JP, Overvatn A, Ishii T, Elazar Z, Komatsu M, Dikic I, Johansen T.** 2009. A role for NBR1 in autophagosomal degradation of ubiquitinated substrates. Mol. Cell **33:**505–516. http://dx.doi.org/10.1016/j.molcel.2009.01.020.
20. **Johansen T, Lamark T.** 2011. Selective autophagy mediated by autophagic adapter proteins. Autophagy **7:**279–296. http://dx.doi.org/10.4161/auto.7.3.14487.
21. **Pankiv S, Clausen TH, Lamark T, Brech A, Bruun JA, Outzen H, Overvatn A, Bjorkoy G, Johansen T.** 2007. p62/SQSTM1 binds directly to Atg8/LC3 to facilitate degradation of ubiquitinated protein aggregates by autophagy. J. Biol. Chem. **282:**24131–24145. http://dx.doi.org/10.1074/jbc.M702824200.
22. **Bjorkoy G, Lamark T, Brech A, Outzen H, Perander M, Overvatn A, Stenmark H, Johansen T.** 2005. p62/SQSTM1 forms protein aggregates degraded by autophagy and has a protective effect on huntingtin-induced cell death. J. Cell Biol. **171:**603–614. http://dx.doi.org/10.1083/jcb.200507002.
23. **Ichimura Y, Kominami E, Tanaka K, Komatsu M.** 2008. Selective turnover of p62/A170/SQSTM1 by autophagy. Autophagy **4:**1063–1066.
24. **Ding WX, Ni HM, Li M, Liao Y, Chen X, Stolz DB, Dorn GW, Yin XM.** 2010. Nix is critical to two distinct phases of mitophagy, reactive oxygen species-mediated autophagy induction and Parkin-ubiquitin-p62-mediated mitochondrial priming. J. Biol. Chem. **285:**27879–27890. http://dx.doi.org/10.1074/jbc.M110.119537.
25. **Kirkin V, McEwan DG, Novak I, Dikic I.** 2009. A role for ubiquitin in selective autophagy. Mol. Cell **34:**259–269. http://dx.doi.org/10.1016/j.molcel.2009.04.026.
26. **Mathew R, Karp CM, Beaudoin B, Vuong N, Chen G, Chen HY, Bray K, Reddy A, Bhanot G, Gelinas C, Dipaola RS, Karantza-Wadsworth V, White E.** 2009. Autophagy suppresses tumorigenesis through elimination of p62. Cell **137:**1062–1075. http://dx.doi.org/10.1016/j.cell.2009.03.048.
27. **Iwata J, Ezaki J, Komatsu M, Yokota S, Ueno T, Tanida I, Chiba T, Tanaka K, Kominami E.** 2006. Excess peroxisomes are degraded by autophagic machinery in mammals. J. Biol. Chem. **281:**4035–4041. http://dx.doi.org/10.1074/jbc.M512283200.
28. **Martinez-Vicente M, Talloczy Z, Wong E, Tang G, Koga H, Kaushik S, de Vries R, Arias E, Harris S, Sulzer D, Cuervo AM.** 2010. Cargo recognition failure is responsible for inefficient autophagy in Huntington's disease. Nat. Neurosci. **13:**567–576. http://dx.doi.org/10.1038/nn.2528.
29. **Wong E, Bejarano E, Rakshit M, Lee K, Hanson HH, Zaarur N, Phillips GR, Sherman MY, Cuervo AM.** 2012. Molecular determinants of selective clearance of protein inclusions by autophagy. Nat. Commun. **3:**1240. http://dx.doi.org/10.1038/ncomms2244.
30. **Linares JF, Duran A, Yajima T, Pasparakis M, Moscat J, Diaz-Meco MT.** 2013. K63 polyubiquitination and activation of mTOR by the p62-TRAF6 complex in nutrient-activated cells. Mol. Cell **51:**283–296. http://dx.doi.org/10.1016/j.molcel.2013.06.020.
31. **Calvo-Garrido J, Escalante R.** 2010. Autophagy dysfunction and ubiquitin-positive protein aggregates in Dictyostelium cells lacking Vmp1. Autophagy **6:**100–109. http://dx.doi.org/10.4161/auto.6.1.10697.
32. **Klionsky DJ, Abeliovich H, Agostinis P, Agrawal DK, Aliev G, Askew DS, Baba M, Baehrecke EH, Bahr BA, Ballabio A, Bamber BA, Bassham DC, Bergamini E, Bi X, Biard-Piechaczyk M, Blum JS, Bredesen DE, Brodsky JL, Brumell JH, Brunk UT, Bursch W, Camougrand N, Ce-**

bollero E, Cecconi F, Chen Y, Chin LS, Choi A, Chu CT, Chung J, Clarke PG, Clark RS, Clarke SG, Clave C, Cleveland JL, Codogno P, Colombo MI, Coto-Montes A, Cregg JM, Cuervo AM, Debnath J, Demarchi F, Dennis PB, Dennis PA, Deretic V, Devenish RJ, Di Sano F, Dice JF, Difiglia M, Dinesh-Kumar S, Distelhorst CW, et al. 2008. Guidelines for the use and interpretation of assays for monitoring autophagy in higher eukaryotes. Autophagy **4:**151–175.

33. **Mizushima N, Yoshimori T, Levine B.** 2010. Methods in mammalian autophagy research. Cell **140:**313–326. http://dx.doi.org/10.1016/j.cell.2010.01.028.
34. **Jackson WT, Giddings TH, Jr, Taylor MP, Mulinyawe S, Rabinovitch M, Kopito RR, Kirkegaard K.** 2005. Subversion of cellular autophagosomal machinery by RNA viruses. PLoS Biol. **3:**e156. http://dx.doi.org/10.1371/journal.pbio.0030156.
35. **N′Diaye EN, Kajihara KK, Hsieh I, Morisaki H, Debnath J, Brown EJ.** 2009. PLIC proteins or ubiquilins regulate autophagy-dependent cell survival during nutrient starvation. EMBO Rep. **10:**173–179. http://dx.doi.org/10.1038/embor.2008.238.
36. **Gamerdinger M, Kaya AM, Wolfrum U, Clement AM, Behl C.** 2011. BAG3 mediates chaperone-based aggresome-targeting and selective autophagy of misfolded proteins. EMBO Rep. **12:**149–156. http://dx.doi.org/10.1038/embor.2010.203.
37. **Hoang B, Benavides A, Shi Y, Frost P, Lichtenstein A.** 2009. Effect of autophagy on multiple myeloma cell viability. Mol. Cancer Ther. **8:**1974–1984. http://dx.doi.org/10.1158/1535-7163.MCT-08-1177.
38. **Schwartz-Roberts JL, Shajahan AN, Cook KL, Warri A, Abu-Asab M, Clarke R.** 2013. GX15-070 (obatoclax) induces apoptosis and inhibits cathepsin D- and L-mediated autophagosomal lysis in antiestrogen-resistant breast cancer cells. Mol. Cancer Ther. **12:**448–459. http://dx.doi.org/10.1158/1535-7163.MCT-12-0617.
39. **Bauer PO, Goswami A, Wong HK, Okuno M, Kurosawa M, Yamada M, Miyazaki H, Matsumoto G, Kino Y, Nagai Y, Nukina N.** 2010. Harnessing chaperone-mediated autophagy for the selective degradation of mutant huntingtin protein. Nat. Biotechnol. **28:**256–263. http://dx.doi.org/10.1038/nbt.1608.
40. **Johnson AJ, Yeh YY, Smith LL, Wagner AJ, Hessler J, Gupta S, Flynn J, Jones J, Zhang X, Bannerji R, Grever MR, Byrd JC.** 2012. The novel cyclin-dependent kinase inhibitor dinaciclib (SCH727965) promotes apoptosis and abrogates microenvironmental cytokine protection in chronic lymphocytic leukemia cells. Leukemia **26:**2554–2557. http://dx.doi.org/10.1038/leu.2012.144.
41. **Settembre C, Di Malta C, Polito VA, Garcia Arencibia M, Vetrini F, Erdin S, Erdin SU, Huynh T, Medina D, Colella P, Sardiello M, Rubinsztein DC, Ballabio A.** 2011. TFEB links autophagy to lysosomal biogenesis. Science **332:**1429–1433. http://dx.doi.org/10.1126/science.1204592.
42. **Su H, Li F, Ranek MJ, Wei N, Wang X.** 2011. COP9 signalosome regulates autophagosome maturation. Circulation **124:**2117–2128. http://dx.doi.org/10.1161/CIRCULATIONAHA.111.048934.
43. **Kimmelman AC.** 2011. The dynamic nature of autophagy in cancer. Genes Dev. **25:**1999–2010. http://dx.doi.org/10.1101/gad.17558811.
44. **Myeku N, Figueiredo-Pereira ME.** 2011. Dynamics of the degradation of ubiquitinated proteins by proteasomes and autophagy: association with sequestosome 1/p62. J. Biol. Chem. **286:**22426–22440. http://dx.doi.org/10.1074/jbc.M110.149252.
45. **Dai Y, Grant S.** 2004. Small molecule inhibitors targeting cyclin-dependent kinases as anticancer agents. Curr. Oncol. Rep. **6:**123–130. http://dx.doi.org/10.1007/s11912-004-0024-3.
46. **Liu J, Xia H, Kim M, Xu L, Li Y, Zhang L, Cai Y, Norberg HV, Zhang T, Furuya T, Jin M, Zhu Z, Wang H, Yu J, Li Y, Hao Y, Choi A, Ke H, Ma D, Yuan J.** 2011. Beclin1 controls the levels of p53 by regulating the deubiquitination activity of USP10 and USP13. Cell **147:**223–234. http://dx.doi.org/10.1016/j.cell.2011.08.037.
47. **Boya P, Gonzalez-Polo RA, Casares N, Perfettini JL, Dessen P, Larochette N, Metivier D, Meley D, Souquere S, Yoshimori T, Pierron G, Codogno P, Kroemer G.** 2005. Inhibition of macroautophagy triggers apoptosis. Mol. Cell. Biol. **25:**1025–1040. http://dx.doi.org/10.1128/MCB.25.3.1025-1040.2005.
48. **Germain M, Mathai JP, Shore GC.** 2002. BH-3-only BIK functions at the endoplasmic reticulum to stimulate cytochrome c release from mitochondria. J. Biol. Chem. **277:**18053–18060. http://dx.doi.org/10.1074/jbc.M201235200.
49. **Chang NC, Nguyen M, Germain M, Shore GC.** 2010. Antagonism of Beclin 1-dependent autophagy by BCL-2 at the endoplasmic reticulum requires NAF-1. EMBO J. **29:**606–618. http://dx.doi.org/10.1038/emboj.2009.369.
50. **Zhu H, Zhang L, Dong F, Guo W, Wu S, Teraishi F, Davis JJ, Chiao PJ, Fang B.** 2005. Bik/NBK accumulation correlates with apoptosis-induction by bortezomib (PS-341, Velcade) and other proteasome inhibitors. Oncogene **24:**4993–4999. http://dx.doi.org/10.1038/sj.onc.1208683.
51. **Lopez J, Hesling C, Prudent J, Popgeorgiev N, Gadet R, Mikaelian I, Rimokh R, Gillet G, Gonzalo P.** 2012. Src tyrosine kinase inhibits apoptosis through the Erk1/2-dependent degradation of the death accelerator Bik. Cell Death Differ. **19:**1459–1469. http://dx.doi.org/10.1038/cdd.2012.21.
52. **Amaravadi RK, Yu D, Lum JJ, Bui T, Christophorou MA, Evan GI, Thomas-Tikhonenko A, Thompson CB.** 2007. Autophagy inhibition enhances therapy-induced apoptosis in a Myc-induced model of lymphoma. J. Clin. Invest. **117:**326–336. http://dx.doi.org/10.1172/JCI28833.
53. **Cho DH, Jo YK, Hwang JJ, Lee YM, Roh SA, Kim JC.** 2009. Caspase-mediated cleavage of ATG6/Beclin-1 links apoptosis to autophagy in HeLa cells. Cancer Lett. **274:**95–100. http://dx.doi.org/10.1016/j.canlet.2008.09.004.
54. **Luo S, Rubinsztein DC.** 2010. Apoptosis blocks Beclin 1-dependent autophagosome synthesis—an effect rescued by Bcl-xL. Cell Death Differ. **17:**268–277. http://dx.doi.org/10.1038/cdd.2009.121.
55. **Wirawan E, Vande Walle L, Kersse K, Cornelis S, Claerhout S, Vanoverberghe I, Roelandt R, De Rycke R, Verspurten J, Declercq W, Agostinis P, Vanden Berghe T, Lippens S, Vandenabeele P.** 2010. Caspase-mediated cleavage of Beclin-1 inactivates Beclin-1-induced autophagy and enhances apoptosis by promoting the release of proapoptotic factors from mitochondria. Cell Death Dis. **1:**e18. http://dx.doi.org/10.1038/cddis.2009.16.
56. **Yousefi S, Perozzo R, Schmid I, Ziemiecki A, Schaffner T, Scapozza L, Brunner T, Simon HU.** 2006. Calpain-mediated cleavage of Atg5 switches autophagy to apoptosis. Nat. Cell Biol. **8:**1124–1132. http://dx.doi.org/10.1038/ncb1482.
57. **Betin VM, Lane JD.** 2009. Caspase cleavage of Atg4D stimulates GABARAP-L1 processing and triggers mitochondrial targeting and apoptosis. J. Cell Sci. **122:**2554–2566. http://dx.doi.org/10.1242/jcs.046250.
58. **Tsvetkov AS, Miller J, Arrasate M, Wong JS, Pleiss MA, Finkbeiner S.** 2010. A small-molecule scaffold induces autophagy in primary neurons and protects against toxicity in a Huntington disease model. Proc. Natl. Acad. Sci. U. S. A. **107:**16982–16987. http://dx.doi.org/10.1073/pnas.1004498107.
59. **Ling J, Kang Y, Zhao R, Xia Q, Lee DF, Chang Z, Li J, Peng B, Fleming JB, Wang H, Liu J, Lemischka IR, Hung MC, Chiao PJ.** 2012. KrasG12D-induced IKK2/beta/NF-kappaB activation by IL-1alpha and p62 feedforward loops is required for development of pancreatic ductal adenocarcinoma. Cancer Cell **21:**105–120. http://dx.doi.org/10.1016/j.ccr.2011.12.006.
60. **Maiuri MC, Criollo A, Kroemer G.** 2010. Crosstalk between apoptosis and autophagy within the Beclin 1 interactome. EMBO J. **29:**515–516. http://dx.doi.org/10.1038/emboj.2009.377.
61. **Wong E, Cuervo AM.** 2010. Integration of clearance mechanisms: the proteasome and autophagy. Cold Spring Harb. Perspect. Biol. **2:**a006734. http://dx.doi.org/10.1101/cshperspect.a006734.
62. **Ma X, Godar RJ, Liu H, Diwan A.** 2012. Enhancing lysosome biogenesis attenuates BNIP3-induced cardiomyocyte death. Autophagy **8:**297–309. http://dx.doi.org/10.4161/auto.18658.